DEMOCRATIC AND POPULAR REPUBLIC OF ALGERIA
Ministry of Higher Education and Scientific Research

Mohamed Khider University-BISKRA.

Faculty of Exact Sciences and Science of Nature and Life

Material sciences department

Memory

Presented for obtaining **Magister Diploma in Physics**

Option: Physics of Materials

By: **Madani BDIRINA**

THEME

SYNTHESIS AND CHARACTERIZATION OF ZINC OXIDE THIN FILMS FOR THE OPTIMIZATION OF A SPRAY DEPOSITION SYSTEM

Commenced in: 13 / 11 / 2012

In front of the jury:

President:	A. CHALA	Prof.	Univ. Biskra
Examiners:	A. ATTAF	Prof.	Univ. Biskra
	H. BEN TEMAM	M.C.	Univ. Biskra
Supervisor:	S. RAHMANE	M.C.	Univ. Biskra

Acknowledgments

I would like to thank my family for their support and encouragement throughout my education and life.

I would like to express my deepest appreciation to my memo advisor Dr. Saad Rahmane for all his great support, guidance and patience throughout my research.

I am also thankful to my reading committee members, Professor Abdelouahed Chala, Professor Abdallah Attaf and Dr. Hachemi Ben Temam for their time to read my memo and for accepting to judge this dissertation.

I would like to thank Professor Mohamed Salah Aida for his assistance in the optical and the electrical measurements in several times and for his counsels.

I would like to thank Mr. Brahim Gasmi for his assistance in XRD and SEM characterizations.

I would like to acknowledge the assistance of my colleagues and lab mates A. Thabet, M. Fezari, S. Leguireh and Z. Khaldi.

I would like to thank my friends Chaiba, Sliman Chala, Khaled Ztaito and Youness Tounsi for their constant support and assistance.

TABLE OF CONTENTS

INTRODUCTION

Introduction

Metal oxide thin films play an important role in many applications due to the wide range covered by their optical, mechanical, structural, chemical and electrical properties. Most of them are characterized by a wide bandgap (>3 eV) and high transparency, while their refractive index, response to an external voltage, conductivity and crystallinity depend on the specific metal oxide. The most widespread applications of the metal oxide thin films, based on each of these properties are: optical coatings (Al_2O_3, TiO_2...) [1], electrochromic windows (WO_3, MoO_3, V_2O_5…) [2, 3], piezoelectric sensors (PZT, ZnO…) [4, 5], gate dielectrics in CMOS devices (SiO_2, Al_2O_3…) [6] and others.

An interesting class of MOs is the Transparent Conductive Oxides (TCOs), which combine the wide bandgap, characteristic to dielectrics, with the low electrical resistivity ($<10^{-3}$ Ωcm), characteristic to metals. They are highly transparent in the visible region and highly reflective in the near infrared. Nowadays the most researched TCOs are tin oxide (SnO_2), indium oxide (In_2O_3) and zinc oxide (ZnO).

In addition to their optoelectronic proprieties, the zinc oxide has many remarkable features such as: mechanical, chemical, thermal, magnetic, piezoelectric, catalytic proprieties, its non-toxicity and low cost fabrication. All these proprieties make it an important material for several applications especially in form of thin films.

The proprieties of ZnO thin films depend on their deposition technologies. Various deposition techniques have been employed to grow polycrystalline zinc oxide thin films such as:

PVD (physical vapor deposition), CVD (chemical vapor deposition).

Regardless of the technique that used in the deposition, the obtained films are extremely sensitive to the elaboration conditions. Among the new explored ways, there is the spray pyrolysis technique (SPD); it is a simple technique, not sophisticated and especially inexpensive.

According to the generation mode of the droplets, this method has the advantage of producing oxide materials with a good homogeneity of deposition on surfaces which can be wide, having a rough aspect and a considerable deposition rates. It has also the advantage of a good control of the doping rate and does not require significant equipment compared with the vacuum deposition methods. All those make it a potential and promised method to produce thin films with good quality.

In this context that our main goal in this research task is the realization and the improvement of an ultrasonic spray pyrolysis system to make it useful for the elaboration of thin films.

According to the literature the deposition of ZnO in thin layers can be carried out by various techniques, but the quality is not always the same, where the properties vary between the more or less definite limits. For the same process, the differences between the properties measured in various laboratories are often appreciable, maybe due to the difference in the controlling parameters.

Therefore the optimization of any deposition system, even in the sophisticated processes, is necessary before any work in order to obtain the best results.

Our work was carried out at the electro-deposition laboratory in University of Biskra. In first time we interested to the improvement of our ultrasonic spray system by combination with pneumatic system, in same time we worked at the adjustment of the deposition parameters in order to realize reproducible deposition. Then we started to optimize the elaboration condition of this new deposition system.

This work also comprises three chapters:

- The first chapter includes a theoretical presentation of the properties of transparent conductive oxides, in particular zinc oxide and its applications in the form of thin films.
- The second chapter includes brief description of some deposition technologies of thin films as well as structural, optical and electric methods of characterization used in this work.
- The third chapter is devoted to the presentation of the technique of deposition per ultrasonic spray pyrolysis and our improvements on it. We interested, thereafter, at the elaboration and the study of the effect of deposition parameters: the flow rate, the distance between the atomizer and the substrate and the air pressure on the physico-chemical properties and optoelectronics of the elaborated films. Thus we determined the optimum values of these elaboration conditions.

Finally we finished, as a conclusion, by summarizing our results and estimating our experimental work.

CHAPITRE I

BASICS ON TRANSPARENT CONDUCTIVE OXIDES TCOs

I.1. Introduction:

The basic Electromagnetic Theory (Maxwell's equations) does not permit a material to be both electrically conducting and optically transparent simultaneously. Optically transparent materials tend to be electrical insulators by virtue of their large band gaps (>3.1 eV). However, Transparent Conductive Oxides (TCOs) is a group of materials with unique physical properties. Despite their large band gaps (>3.1 eV), the TCOs show electrical conductivity of the order of 10^4 S cm^{-1}.

The history of TCO starts from 1907, with the discovery of Cadmium Oxide (CdO) thin film by a German scientist *Karl Baedeker* [1]. Due to small bandgap, transparency of CdO was too low to be used for practical applications. The practical use of TCO started with discovery of tin-doped In_2O_3 in 1954 by *G. Rupprecht* [2]. In 1960s, it was recognized that thin films composed of binary compounds such as ZnO, SnO_2, In_2O_3 and their alloys were also TCOs [3]. In addition to binary compounds, the ternary compounds such as Cd_2SnO_4, $CdSnO_3$ and $CdIn_2O_4$ were developed as TCO materials prior to 1980. In 1980s, impurity-doped ZnO such as ZnO:Al and ZnO:Ga along with abundant of binary compounds were developed. In 1990s, new TCO materials consisting of multicomponent oxides, like combination of ZnO, CdO, In_2O_3 and SnO_2, have been developed [4]. Among all these TCO materials the tin-doped indium oxide commonly known as indium tin oxide (ITO) offers the best available performance in terms of electrical conductivity and optical transparency along with excellent environmental stability, reproducibility and good surface morphology [5]. However, due to rarity and high price of indium the ITO cannot remain in continuous commercial use for device application [6, 7]. All the TCOs mentioned above are just some of the TCO materials reported so far. All these TCOs have electrons as majority charge carriers and hence known as n-type TCOs. There was no p-type TCO reported until 1993, when *H. Satu and his co-workers* reported NiO as p-type TCO [8]. The second report on $CuAlO_2$ as a p-type TCO was published in 1997, by *H. Kawazoe et al.,* with considerable improvements over NiO [9]. This opened the development of a series of p-type TCOs [10]. However, until now no efficient p-type TCO having optoelectrical properties comparable to its n-type counterpart is available. If there would be an efficient p-type TCO, it can be used as alternative to ITO along with the fabrication of transparent pn-

junction which will lead to a new generation of electronics known as "transparent electronics".

In the literature there are many interesting reviews which summarize all published works as well as a very complete study of the properties of these materials and their methods of preparation in last decades such as *Vossen* [11], *Haacke* [12], and *Chopra et al* [13].

I.2. Electrical Conductivity:

TCOs may be n or p-type semiconductors depending upon their charge carrier generation mechanism. The conductivity of n-type TCOs is always higher than that of p-type due to relative small effective mass of electron in conduction band than that of hole in the valence band.

The most widely used TCOs are n-type with the *Fermi* level within the conduction band. They are conductive and behave like metals. In this case, the materials are called degenerate semiconductors; the free electron gas model of solids applies. The resistivity ρ and conductivity σ are given by:

$$\rho = \frac{1}{\sigma} = \frac{1}{e\,N\,\mu} = \frac{m}{N\,e^2\,\tau} \qquad (1.1)$$

Where N is the free carrier density, $\mu = e\tau/m$ their mobility, e is the charge of the electron, m their effective mass and τ is the relaxation time between two scattering events.

Therefore to obtain a material with high electrical conductivity; high carrier concentration and mobility are essential.

The onset of degeneracy (for n-type) usually takes place at a carrier concentration of around $10^{18}cm^{-3}$ [14, 15]. This is achieved in TCO by either crystal defects (such as oxygen vacancies and/or metal interstitials) or by incorporating extrinsic dopant elements in the crystalline network. The defects and the dopants act as shallow donor levels.

In order to avoid a significant deformation of the crystal lattice, it is necessary that the ionic diameter of the introduced atom is as close as possible to that of the substituted atom. These impurities are generally of valence immediately above (lower for the doping of the type p) than that of the substituted atoms. Each one of these atoms impurities provides a free electron and is thus regarded as an atom donor [16].

However, attempt to place a larger number of dopant atoms in the lattice decreases the mobility due to increase in charge carriers scattering by ionized dopant atoms [17].

Furthermore there are various scattering events determine the mobility of the electrons. For bulk single crystalline TCO, the main scattering processes are the following [18, 19, 20]:

♦ ***Optical phonon scattering:*** caused by the interaction of the electrons with the electric field induced by electric polarization associated with the lattice vibration at optical frequencies.

♦ ***Acoustic phonon scattering:*** caused by the interaction of the electrons with the lattice deformations those correspond to pressure waves.

♦ ***Piezoelectric scattering:*** caused by the interaction of electrons with the electric fields produced by the strain associated with phonons in the crystal.

♦ ***Neutral impurity scattering:*** caused by the interaction of the electrons with uncharged defects.

♦ ***ionized impurity scattering:*** due to deflection of free carriers by the potential of a charge center originating from doping impurities. As TCO are usually heavily doped.

This scattering mechanism is generally predominant. Each scattering mechanism is described with its own scattering relaxation time τ_i and mobility μ_i.

The total scattering relaxation time τ_{Bulk} and the total mobility μ_{Bulk} for the material is deduced by applying Matthiessen's rule to the individual scattering relaxation times τ_i and mobility μ_i:

$$\frac{1}{\tau_{Bulk}} = \sum_i \frac{1}{\tau_i} \quad (1.2) \qquad \frac{1}{\mu_{Bulk}} = \sum_i \frac{1}{\mu_i} \quad (1.3)$$

All the scattering phenomena described previously are related to the bulk single crystal material. However, thin film TCOs are usually polycrystalline. In this case, an additional scattering mechanism occurs due to presence of grain boundaries: the grain boundary scattering. Grain boundaries are present in thin film TCO due to polycrystalline nature of the film induced by the fabrication process.

As described by *Seto* in the case of polycrystalline silicon [21], acceptor centers are localized in grain boundaries, which capture electrons from the conduction band. The grain boundaries are charged negatively and a space charge region extends into the crystallite forming a "back-to-back" *Schottky* potential barrier [21, 22, 23].

I.3. Optical Transparency:

The optical properties of a material depend on the interaction of the electromagnetic wave with the electrons of material. These properties such as transmission (*T*), reflection (*R*), and absorption (*A*), are determined by its refractive index (*n*), extinction coefficient (*k*), band gap energy (*Eg*) and geometry. Geometry includes film thickness, thickness uniformity and film surface roughness.

In principle, we can calculate the optical spectra (i.e. *R*, *T* and *A* as a function of the incoming light frequency) knowing the dielectric function of a material [24]. However, the most critical and difficult issue is to model the dielectric function itself.

The *Drude* dielectric function (is founded on the approximation of the free electron, in a metal) [25] is not valid for the whole electromagnetic spectrum. Therefore, many dielectric function models can be used and even different models can be associated to fit experimental data over a broad frequency range.

In the near infrared region, the *Drude* model is well suited for the description of TCO optical properties. For the UV-visible region, the most commonly used optical models are *Lorentz*, *Cauchy*, *Sellmeier*, *Tauc-Lorentz* and *Forouhi-Bloomer* [26, 27, 28, 29].

Figure.1.1. shows the typical calculated reflectance, transmittance and absorptance curves of a TCO using the *Drude* model (for describing the infrared behavior) in addition to a *Lorentz* oscillator (in order to describe the band gap absorption):

$$\varepsilon(\omega) = \varepsilon_\infty - \frac{\omega_N^2}{\omega^2 + i\,\Gamma\omega} + \frac{\Omega_N^2}{\Omega_0^2 - \omega^2 - i\,\Omega_\Gamma\omega} \quad (1.4)$$

Where ε_∞ is the high frequency dielectric function, $\Gamma = 1/\tau$ is the damping frequency (τ is the *Drude* scattering time) and ω_N^2 is the unscreened plasma frequency of the *Drude* component, Ω_Γ, Ω_N and Ω_0 are the damping frequency, the plasma frequency, and the resonant frequency of the *Lorentz* oscillator. The model considers a finite TCO layer deposited on a glass substrate. The model parameters which used to get typical TCO optical spectra listed in table.1.1.

Where ω_N the unscreened electrons plasma frequency defined by:

$$\omega_N^2 = \frac{N_{optic}\, e^2}{\varepsilon_0 m} \quad (1.5)$$

Where N is the free electron density, e the electron charge, ε_0 the permittivity of free space and m the electron effective mass. With analogy with equation.1.6, the optical mobility μ_{optic} is given by:

$$\mu_{optic} = \frac{e}{\Gamma m} \quad (1.6)$$

It is noticeable that electrical parameters such as the free electron density N_{optic} and the carrier mobility N_{optic} are present in the dielectric function.

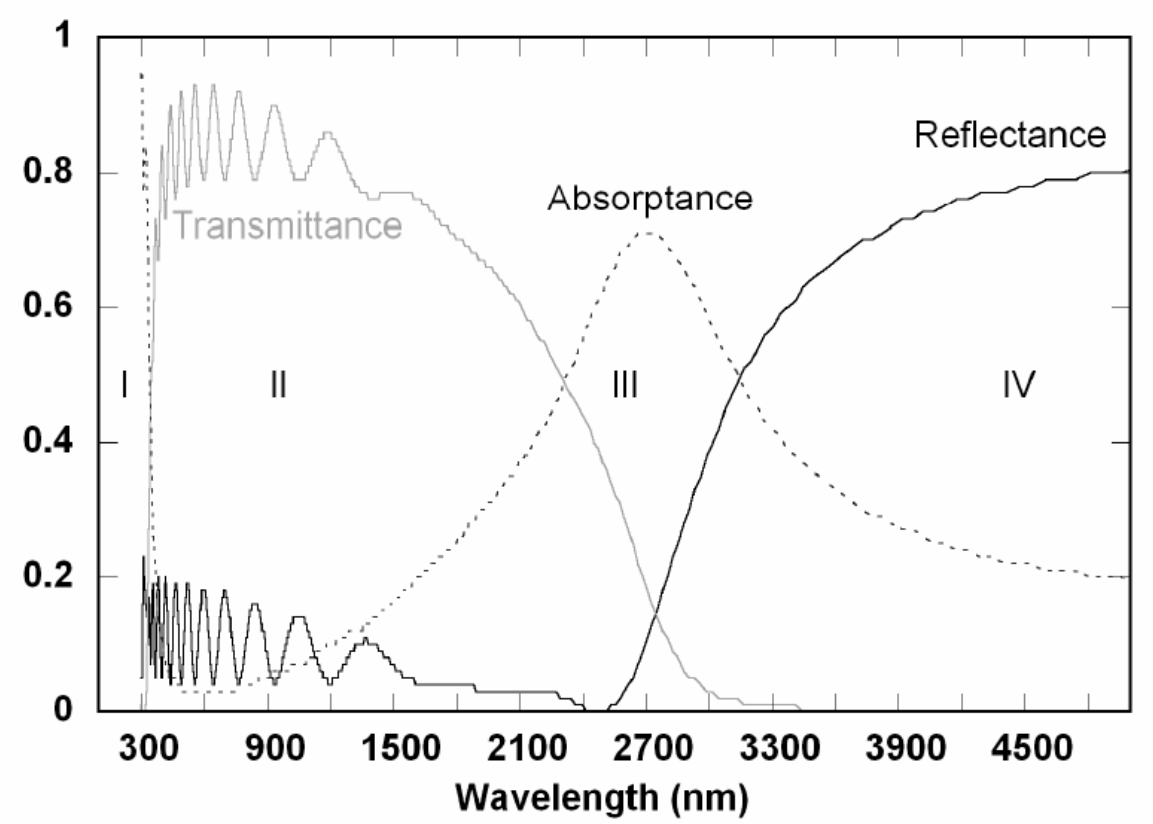

Figure 1.1. *The calculated transmittance, absorptance and reflectance for a typical TCO* [30].

Thickness (µm)	$\varepsilon_\infty\ (cm^{-1})$	$\omega_N\ (cm^{-1})$	$\Gamma(cm^{-1})$	$\Omega_N(cm^{-1})$	$\Omega_0(cm^{-1})$	$\Omega_I(cm^{-1})$
1	3.8	7000	475	11000	32000	800

Table.1.1: *The parameters of the Drude + Lorentz oscillator model used to obtain the optical spectra of figure 2.2* [30].

Four separate regions come into view in these spectra; they are labeled with roman numbers on figure .1.1.

- In the UV region, i.e. region I, the band gap absorption takes place.
- In the visible and near-IR regions, i.e. region II, the TCO are transparent.

Several factors limit the transmission in this region: Firstly, the reflection losses at the optical interface; secondly, the residual absorption, primarily due to free carrier but also to material defects. Finally, interference phenomena take place depending of the thickness of the layer.

♦ In the infrared region the *Drude* model explains the optical properties leading in region III mostly to free carrier absorption and in region IV mostly to free carrier reflection.

The optical bandgap widening or shrinkage is generally attributed to the doping level. The optical bandgap widening is due to the optical band filling effect above the critical *Mott* carrier density: a well-know *Burstein-Moss* effect. This effect is usually attributed to the occupation of conduction band, inducing optical transitions at energies higher than the fundamental electronic gap. The optical shrinkage is due to electron-electron interaction and higher carrier concentration i.e., in this case, donor level approaches the conduction band [31–32]. For a material to be transparent, not only a wide fundamental bandgap is important, but there should be no visible light transition between occupied-unoccupied states inside CB and VB [33].

I.4. Zinc Oxide ZnO :

I.4.1. Introduction

Zn is more abundant than In and Sn (94 ppm compared with 0.1 ppm and 2 ppm, respectively) and less toxic than Cd, which makes ZnO a desired alternative for the most common used TCOs at the moment, i.e., indium tin oxide (In_2O_3:Sn, ITO), fluorine doped tin oxide (SnO_2:F) and cadmium stannate (Cd_2SnO_4).

ZnO occurs naturally as the mineral zincite. However, most ZnO used commercially is synthetically produced. ZnO is widely used as an additive in a variety of applications including ceramics, plastics, cement, glasses, lubricants, paints, pigments, and ointments. Recently, due to its semiconducting properties, ZnO has been very attractive to researchers as an emerging material for electronics applications. In this chapter, a brief review of the structural, optical and electronic properties of ZnO thin films relevant to its microelectronics applications is presented.

I.4.2. The Structure of ZnO:

Most of the group II–VI binary compound semiconductors crystallize in either cubic zinc blende or hexagonal wurtzite structure where each anion is surrounded by four cations at the corners of a tetrahedron, and vice versa. This tetrahedral coordination is typical of sp^3 covalent bonding nature, but these materials also have a substantial ionic character that tends to increase the bandgap beyond the one expected from the covalent bonding. ZnO is a II–VI compound semiconductor whose ionicity resides at the borderline between the covalent and ionic semiconductors. The crystal structures shared by ZnO are wurtzite, zinc blende, and rocksalt (or Rochelle salt) as schematically shown in Figure 1.2.

Under ambient conditions, the thermodynamically stable phase is that of wurtzite symmetry. The zinc blende ZnO structure can be stabilized only by growth on cubic substrates, and the rocksalt or Rochelle salt (NaCl) structure may be obtained at relatively high pressures, as in the case of GaN [20].

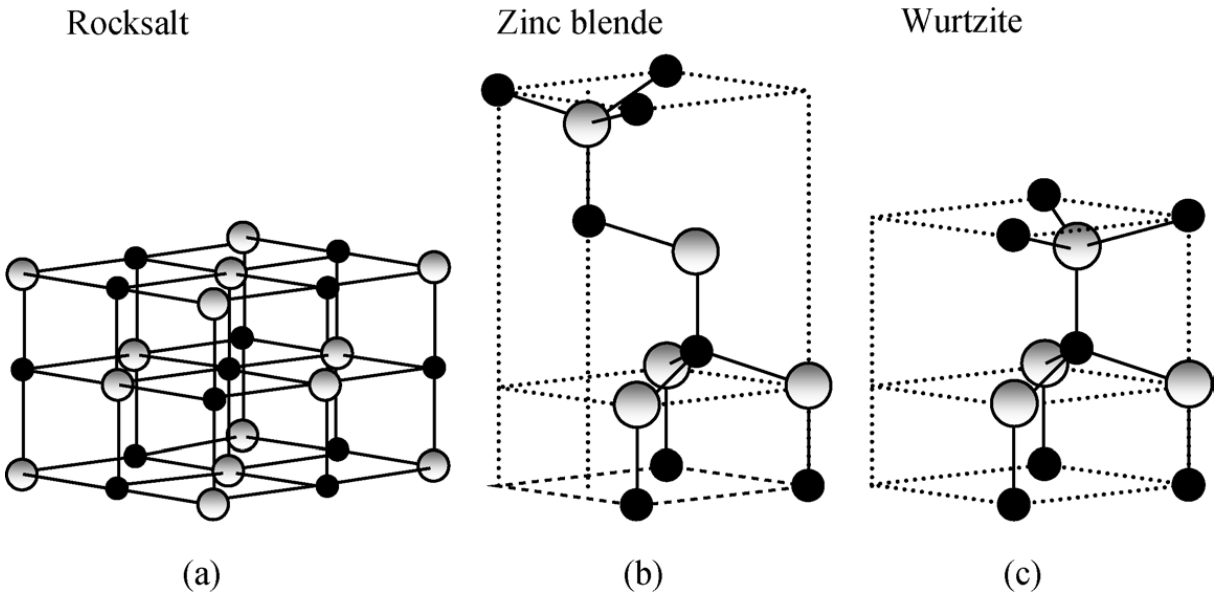

Figure 1.2 *Stick-and-ball representation of ZnO crystal structures: (a) cubic rocksalt , (b) cubic zinc blende , and (c) hexagonal wurtzite . Shaded gray and black spheres denote Zn and O atoms, respectively.*

The wurtzite structure has a hexagonal unit cell with two lattice parameters a and c in the ratio of c/a = $\sqrt{(8/3)}$= 1,633; (in an ideal wurtzite structure) and belongs to the space group C_{6v}^4 in the *Schoenflies* notation and *P6₃mc* in the *Hermann–Mauguin* notation. A schematic representation of the wurtzitic ZnO structure is shown in Figure 1.3. The structure is composed of two interpenetrating hexagonal closepacked (hcp) sublattices, each of which consists of one type of atom displaced with respect to each other along the threefold c-axis by the amount of u= 3/8= 0.375 (in an ideal wurtzite structure) in fractional coordinates. The internal parameter u is defined as the length of the bond parallel to the c-axis (anion–cation bond length or the nearest-neighbor distance) divided by the c lattice parameter. The basal plane lattice parameter (the edge length of the basal plane hexagon) is universally depicted by a; the axial lattice parameter (unit cell height), perpendicular to the basal plane, is universally described by c. Each sublattice includes four atoms per unit cell, and every atom of one kind (group II atom) is surrounded by four atoms of the other kind (group VI), or vice versa, which are coordinated at the edges of a tetrahedron. The crystallographic vectors of wurtzite are: $\vec{a}$ = a (1/2,$\sqrt{3}$/2, 0), $\vec{b}$ = a (1/2, -$\sqrt{3}$/2, 0), and $\vec{c}$ = a (0, 0, c/a). In Cartesian coordinates, the

basis atoms are (0, 0, 0), (0, 0, uc), a (1/2, $\sqrt{3}$/6, c/2a), and a (1/2, $\sqrt{3}$/6, [u+1/2] c/a) [35].

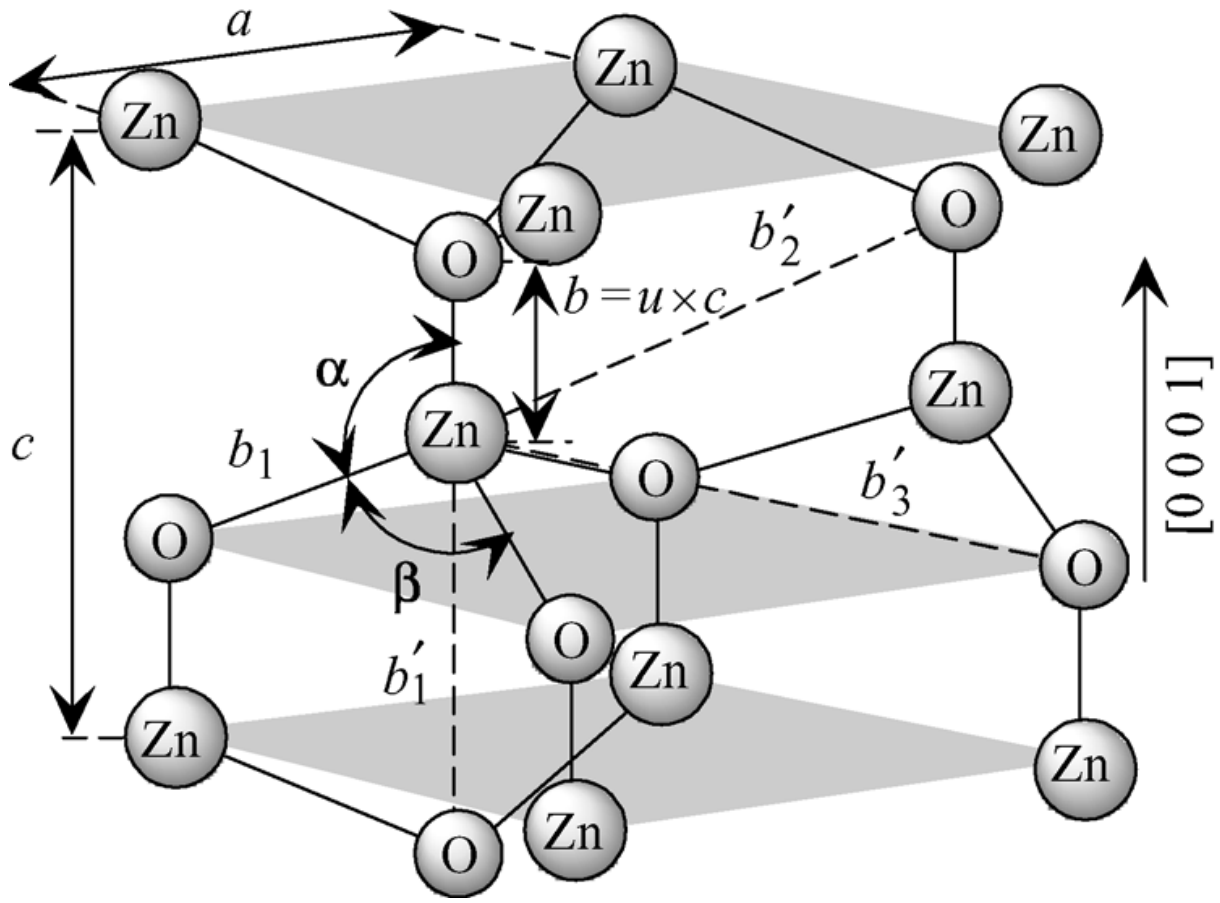

Figure.1.3: *Schematic representation of a wurtzitic ZnO structure with lattice constants a in the basal plane and c in the basal direction, u parameter, which is expressed as the bond length or the nearest-neighbor distance b divided by c (0.375 in ideal crystal), α and β (109.47 in ideal crystal) bond angles, and three types of second-nearest-neighbor distances b_1', b_2' and b_3'.*

I.4.3. Electrical Properties of ZnO:

Zinc oxide is a II-VI wide and direct bandgap (~3.4 eV) semiconductor. According to the mode of preparation and the rate of doping, the value of forbidden band and consequently the electric properties can be largely modified.

The dominating n-type character in ZnO has often been attributed to the presence of intrinsic native defects (O vacancies (V_0) and/or Zn interstitials

(Zn_i)). The reactions for creating excess electron carriers can be expressed as in equation (1.2); for V_0 and Zn_i respectively:

$$ZnO \rightarrow ZnO_{(1-X)} + xV_0^+ + x\left[\frac{1}{2}O_2(g)\right] + xe^- \qquad (1.7a) \quad with \quad x < 1$$

$$ZnO \rightarrow (1-x)\,ZnO + xZn_i^+ + x\left[\frac{1}{2}O_2(g)\right] + xe^- \qquad (1.7b) \quad with \quad x < 1$$

However, there is still a great deal of controversy over which of these two defects is the dominant cause of the n-type character [36]. Some researchers have suggested that V_0 are deep-level states [37, 38] and Zn_i occur as shallow donors (~25 – 30 meV below conduction band) [39].

Therefore V_0 are not likely to be the dominant cause of n-doping in undoped ZnO films.

I.4.4. Doping in ZnO:

I.4.4.1. *n*-type doping:

In order to extrinsically dope ZnO n-type, Zn or O atoms are usually substituted with an atom that has one valence electron more than the atom it replaces. Thus, group III elements are potential shallow donors on Zn cation sites. Recent reports have demonstrated that boron (B), aluminum (Al), gallium (Ga), indium (In), and fluorine (F) -doped ZnO films can be achieved [40, 41, 42, 43, 44], exhibiting both low resistivity and high transparency in the visible region. Once degenerate doping has been achieved, excess doping does not move the Fermi level any further and only contributes to mobility degradation via impurity and grain boundary scattering (as excess metallic ions segregate into the grain boundaries and are not activated) [45]. It has been predicted that ionized impurity scattering is the major limitation to degenerate doping in oxide semiconductors, limiting the carrier concentration to below 2×10^{21} cm $^{-3}$ [46, 47].

I.4.4.2. *p*-type doping:

In this case must be substitute Zn or O atoms by group I elements or group V elements respectively.

The substitution of a Zn cation site with group I elements (lithium (*Li*), sodium (*Na*), potassium (*K*), silver (*Ag*), and copper (*Cu*)) should result in the creation of acceptor states that would induce p-type conductivity [48, 49, 50]. This has however been difficult to achieve due to the large density of back-ground compensating states and partly due to the fact that the acceptor states obtained by Zn-site substitution are usually deep levels at room temperature (with activation energies of a few hundred meV, much greater than k_BT at room temperature). In addition, excess impurity atoms occupying the interstitial sites will act as donors, compensating part of the acceptors and also inducing more disorder. As a consequence of these issues, attempts have been made to achieve p-type conductivity via substitution with group V elements (N, P, As, and Sb) at the O-anion sites [51]. Many reports indicate that this may be the only route to achieving p-type conductivity (although the carrier concentration is limited to less than 10^{18}), and N has been most promising in this regard (this maybe due to its close atomic radius to that of the O-atom) [52-53].

I.4.5. Optical properties and luminescence of ZnO:

The large optical bandgap (~3.4 eV) of ZnO makes ZnO highly transparent to visible light, its refractive index in the massive form is equal to 2. In the form of thin film, its refractive index and its absorption coefficient vary according to the elaboration conditions. The refractive index has a value which varies between 1,90 and 2,20 following the authors. The improvement of ZnO stoechiometry leads to a reduction in the absorption coefficient and to an increase in the energy of the forbidden band. The doped zinc oxide classified in TCO. Very little doped, it can be used in luminescence [54].

ZnO exposed under an electromagnetic beam or an electrons beam of high energy (E > 3.4 eV) emits photons, so called: luminescence phenome-

non. According to the elaboration conditions and subsequent treatments, various bands of photoluminescence were observed in: the near UV (350 nm), and the visible (green color radiation of wavelength close to 550 nm). In stoechiometric ZnO thin films, the visible luminescence is due to the defects which are related to deep level emissions, such as zinc interstitials and oxygen vacancies [55]. *Fons et al.* [56] reported that the study of the photoluminescence properties of films in the visible region can provide informations on quality and purity of material.

The most desirable feature of zinc oxide is to have the largest exciton binding energy of 60 meV as compared to 24 meV for GaN, which is the key parameter that enables the UV laser diode and other exciton related light emitting devices to be operated at room temperature and makes ZnO a brighter emitter. Unlike GaN, ZnO can be grown in bulk, at lower temperature than it, also compatible with wet etchants and does not need dry etching [57].

1.4.6. Applications of ZnO:

Zinc oxide has been used in many fields over the years, from rubber and concrete industries to medicine and cosmetics. More recently, ZnO has been implemented in TCO applications, such as solar cells, liquid crystal displays (LCDs), or heat protecting windows.

Other advantages of ZnO are the resistance to high energy radiation, which makes it suitable for space applications, as well as the stability and amenability to wet chemical etching, which can be exploited for the fabrication of small size devices. Moreover, the high exciton binding energy (60 meV), makes it a strong candidate for UV light emitters.

ZnO single crystals with mobility up to 200 cm^2/Vs have been obtained by several groups recently, using vapor-phase, pressurized melt and hydrothermal techniques. The availability of high quality ZnO substrates opened new possibilities for growing high quality epitaxial GaN, a III-V semiconductor commonly used in UV lasers and diode applications [58], which has a very small lattice mismatch, of about 2%, with ZnO.

Zinc oxide also proved to be a promising gas sensor, due to the reversible changes encountered by its surface conductivity upon exposure to different gases. Studies performed on ZnO as sensor for combustible gases (H_2 [59], liquid petroleum gas-LPG [60], CH_4 [61]), toxic gases (CO [62], H_2S [61], NO_x [63]) have been reported.

Another interesting class of materials is formed by the dilute magnetic semiconductors (DMS), which have been thoroughly studied in the last years due to their potential in the spintronics field. DMSs refer to III-V compounds (GaN, GaAs, AlN etc.) and II-VI materials (CdTe, ZnSe, CdSe, CdS etc.).

Among the last ones, ZnO has received special attention since the predictions of *Dietl* [64]. Ferromagnetism was obtained by doping zinc oxide with various transition metals, such as Mn, Co, V, Sc, Ti, Ni, Cr, Fe or Cu. Despite the considerable efforts put in these studies, the exact causes for ferromagnetism in ZnO are still not known, since also contradictory results for the Curie temperature have been reported.

A hot topic in the past few years has arisen from the extraordinary ability of ZnO to self-assemble into nanostructures. In only few years a large variety of nanocrystalline ZnO structures have been reported, such as wires, rods, walls, belts, combs, springs, spirals, tetrapods and even cages. The ZnO nanostructures can be used in (nano) sensors [65], field effect transistors (FETs) [66], lasing [67], hybrid solar cells [68, 69], or for manufacturing AFM cantilevers [70]. The techniques used for obtaining the ZnO nanocrystalline structures, both catalyst-assisted, such as a vapor-liquid-solid (VLS) growth method and molecular beam epitaxy (MBE) or catalyst-free, such as MOCVD, aqueous solution growth, and electrodeposition.

The table below summarizes some properties of wurtzite ZnO:

Lattice parameters at 300 K	
a	0.32495 nm
c	0.52069 nm
c/a	1.602 (ideal hexagonal structure shows 1.633)
u	0.345
Density (gcm^{-3})	5.606
Stable phase at 300 K	Wurtzite
Melting point (^0C)	1975
Static dielectric constant	8.656
Refractive index	2.008
Energy gap	~ 3.4 eV, direct
Intrinsic carrier	concentration : max n-type doping ~ 10^{20} cm^{-3}; max p-type doping ~ 10^{17} cm^{-3}
Exciton binding energy	60 meV, sufficiently larger than thermal energy at room temperature (~26 meV).
Electron effective mass	0.24
Electron Hall mobility at 300 K for lightly doped n-type ZnO	200 cm^2V^{-1} s^{-1}
Hole effective mass	0.59
Hole Hall mobility at 300 K for lightly doped p-type ZnO	5–50 cm^2V^{-1} s^{-1}

Table.1.2: Properties of wurtzite ZnO [71].

CHAPITRE II

THIN FILM DEPOSITION AND CHARACTERZATION TECHNIQUES

II.1. Thin Film Deposition Methods:

Thin film deposition is the process of adding a thin layer of one material on another. The underlying material on which the layer is added is known as substrate and the layer itself is called thin film. Thin films have become a significant part of micro-electronic circuitry because of their small thickness, i.e. a nearly two-dimensional structure, which permits the fabrication of very small devices or microcircuits [72]. Thin film technology is based on three foundations; fabrication, characterization and applications [73]. Thin films are used for electronic components, electronic displays, optical coatings, magnetic data storage, optical data storage, anti-static coating and hard surface coatings, etc. There are dozens of thin film deposition techniques for various applications. Thin film deposition techniques can be conveniently divided into two classes; (1) Physical Vapor Deposition and (2) Chemical Vapor Deposition. However, a considerable number of deposition techniques combine both physical and chemical processes as-well [74].

The common steps to all techniques of film deposition are:

1. Generating a supply of atoms or molecules from a source that may be solid, liquid or vapor. This is done by supplying energy to the source by heating, by kinetic energy from incident energetic particles or by using chemical reaction to produce volatile species.
2. Transport of the constituent atoms or molecules to the substrate. From a technological point of view, this is the crucial part of a deposition, because the manner of transport determines the quality of the film.
3. Deposition of atoms or molecules on the substrate. The condition of the substrate surface plays important role in this part of the deposition process. If the substrate surface is contaminated with a fraction of monolayer of impurity atoms, the surface mobility of the arriving atoms may be effected to an extent that the crystal orientation of the film bears little relationship to that of the substrate, and the structure is likely to be polycrystalline. Conversely, if the substrate surface is essentially clean, the arriving atoms are likely to adsorb on sites related to substrate orientation, and the film may be preferentially oriented or even epitaxial.

4. Post-deposition treatment. In this part of the process, a prolonged annealing of the film at elevated temperature may yield a film with superior properties as a result of crystal grain growth in the film, stress reduction, the changes in composition produced by diffusion of constituents, etc.
5. Process analysis. Modern in-situ analytical techniques are used to monitor the deposition or post-deposition parameters in order to improve quality of the film in term of structure or purity, or both [72].

II.1.1. Physical Vapor Deposition Techniques:

Physical vapor deposition technique is the transfer of atoms and molecules from a source to a substrate by a process that relies on physical methods to produce the vapor species. Physical vapor deposition is carried out in high vacuum to avoid contamination of the film by ambient atmosphere [72]. Some common and well-known physical vapor deposition techniques are:

II.1.1.1. Pulsed Laser Deposition (PLD):

This technique is based on physical vapor deposition processes arising from the impact of high-power short pulsed laser irradiation of solid targets that leads to the removal of material from the focused zone [75]. PLD is relatively new but very efficient technique to deposit epitaxial films. It is a somewhat costly process, but can produce high quality films with high accurate thickness control [76]. However, reproducibility, large area deposition and reduction of particulate emission have yet to be improved [75].

II.1.1.2. Sputtering:

This technique relies on the removal of atoms from the target by bombarding the target surface with high energetic particles. The target, which is called cathode, is the material to be deposited and substrate is referred to as anode [75]. Sputtering is relatively cost-effective compared with PLD and large area deposition is possible by this process [76].

II.1.1.3. Thermal Evaporation:

This process comprises evaporating source materials in a vacuum chamber and condensing the evaporated particles on a substrate. Thermal evaporation is conventionally called vacuum deposition. Resistive heating is commonly used in this deposition; therefore this technique cannot be applied to high melting point materials and poor thermal conductors [77, 78].

II.1.1.4. Electron Beam Evaporation:

This technique is an improvement over thermal evaporation in which a preheated target is bombarded with a highly accelerated beam of electrons in order to vaporize the target. Source electrons as well as secondary electrons trapping and electron beam arcing are the problems associated with this technique [78].

II.1.1.5. Molecular Beam Epitaxy (MBE):

This process is based on the deposition of thermal beam of atoms or molecules on the clean surface of a single-crystalline substrate held at high temperature under ultra high vacuum conditions to form an epitaxial film [79]. MBE is a sophisticated and finely controlled method for growing single-crystal epitaxial films in high vacuum. Limitations of MBE are the expensive equipment and its complex operation [74].

II.1.2. Chemical Deposition Techniques

A deposition technique, in which chemical components react on the surface of the substrate to form a solid film is called chemical deposition technique [80]. In contrast to physical deposition technique, the chemical deposition often utilizes inert gases and may be carried out at atmospheric pressure [72]. Some of the commonly used chemical deposition techniques are:

II.1.2.1. Chemical Vapor Deposition (CVD):

The process by which the non-volatile products of a gas phase reaction are allowed to deposit onto a substrate is known as chemical vapor deposition [81]. The main feature of CVD is its versatility for synthesizing both simple and complex compounds with relative ease. Fundamental principles of CVD encompass an interdiscipli-

nary range of gas-phase reaction chemistry, thermodynamics, kinetics, transport mechanisms, film growth phenomena and reactor engineering [74]. The advantages of CVD include high deposition rate, low price and flexibility in composition control. However, due to high deposition temperature, CVD is not suitable for substrates which are thermally unstable at high temperatures [82].

II.1.2.2. Spin Coating:

Spin coating process consists of putting the drops of liquid precursor on the surface of a spinning substrate [83]. The film formed on the substrate results from two balancing forces: the centrifugal force (due to spinning) which drives the viscous sol radially outwards and viscous force (due to friction) which acts radially inwards [84]. Spin coating is the cheapest film production method in silicon technology [85]. However, thinner films (<100 nm) are hard to make and can waste 98% of the process materials [86].

II.1.2.3. Dip Coating:

Dip coating or immersion coating is a simple old way of thin film deposition by immersing a substrate in the solution of the coating material at a constant speed (preferably judder free). Film thickness is set by the competition among viscous force, capillary (surface tension) force and gravity. Thickness and uniformity can be sensitive to flow conditions of the substrate in the liquid bath and gas overhead. The withdraw speed of the substrate, the thicker of the film deposited. Theoretical prediction of process performance is more difficult, and the control of the process more demanding [87].

II.1.2.4. Spray Pyrolysis (SP):

In this deposition technique, liquid precursors are sprayed by atomization processes and condensed by thermal decomposition on substrates maintained at elevated temperatures. The sprayed micro-droplets reaching the hot substrate surface undergo pyrolytic decomposition and form a single crystallite or a cluster of crystallites of the sprayed materials. Spray pyrolysis was used as early as 1910 to obtain transparent oxide films [88].

II.1.2.4.1. Classification of Spray Pyrolysis Techniques:

Classification of different spray processes could be made in one way based on the type of energy source for the precursor reaction such as spray pyrolysis in a tubular reactor (SP), vapor flame reactor (VFSP), the emulsion combustion method (ECM) and flame spray pyrolysis (FSP) or the method of atomizing the precursor, namely air pressurized, electrostatic and ultrasonic spray pyrolysis [89]. In the case that the energy source for precursor reaction is an external energy supply and not from the spray itself, (as in SP and VFSP), method is less sensitive to the choice of precursors and solvent. Different types of solvents are used in spray pyrolysis depending on the type and solubility of the precursors and economic aspects. Nitrates, chlorides and acetates are typically chosen as the metal-oxide precursors that can be dissolved in aqueous and alcoholic solvents [88].

The other classification for the type of spray pyrolysis is usually attributed to the type of the atomizer that is used in the system. Also, the droplet size of the aerosol is generally dependent on the atomization method, which in turn determines the film quality. There are three major types of atomizers: air blast, electrostatic, and the ultrasonic. The spray pyrolysis technique using the electrostatic atomizer is called Electrostatic Spray Deposition (ESD), the technique using the air blast atomizer is named Pressurized Spray Deposition (PSD), and the technique using Ultrasonic atomizer is generally recognized as the ultrasonic or normal Spray Pyrolysis (SP).

Atomizer	Droplet size (μm)	Atomization rate (cm^3/min)
Pressure	10-100	3-no limit
Ultrasonic	1-100	<2
Electrostatic	0.1-10	0.5-5

Table.2.1: *Characteristics of atomizers commonly used in spray pyrolysis* [90].

Ultrasonic atomization relies on an electromechanical device that vibrates at a very high frequency. Only low-viscosity Newtonian fluids could be atomized by passing over the vibrating surface and the vibration causes the fluid to break into droplets. Figure.II.1. shows an example of ultrasonic atomization technology.

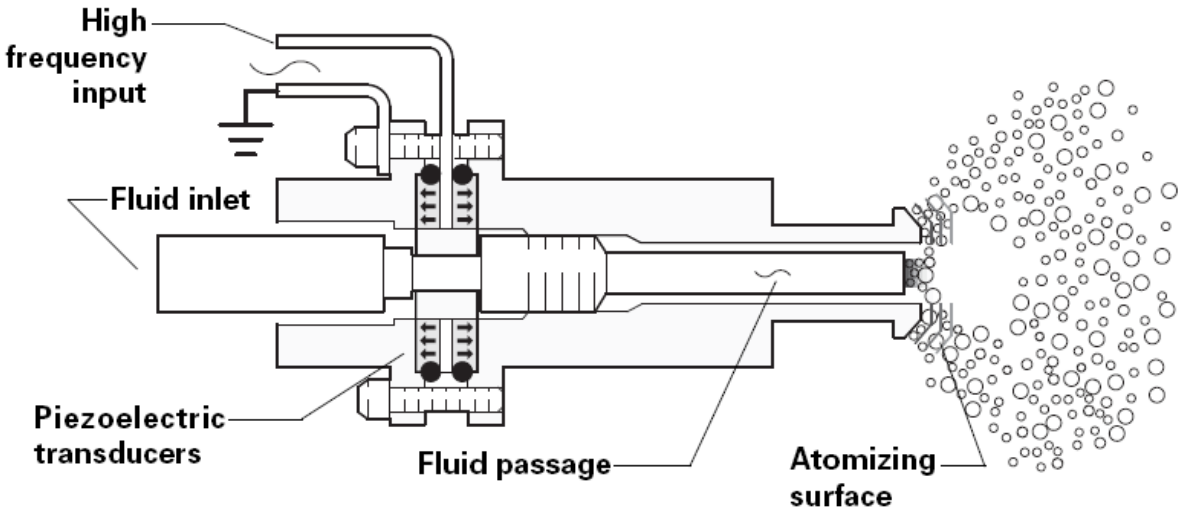

Figure 2.1: *Schematic of an ultrasonic atomizer.*

II.1.2.4.2. Advantages of Spray Pyrolysis:

In comparison with other thin film deposition methods, spray pyrolysis has many advantages including: open-atmosphere process, open reaction chamber, easy access to observe the deposition process and adjustment during the experiment. It has also the multi-layer fabrication capability which is very attractive for making functionally graded films. The composition of the film can be adjusted by changing the precursor solutions. Films can be also obtained on large surfaces. Spray pyrolysis is of great practical interest in processing dense and porous films, by optimizing the deposition variables such as: deposition temperature, substrate temperature, precursor composition and concentration, solvent composition, solution flow rate, carrier gas ratio and flow rate, etc. One of the major advantages of spray pyrolysis over the vapor-phase routes is the possibility of producing multicomponent particles with exact desirable stoechiometry in the final product. Depending on the substrate temperature, precursor type, and the nozzle-to-substrate distance the droplets can evaporate or decompose completely before reaching the substrate, resulting in a process resembling to CVD, or the liquid is deposited without evaporation. Burning a flammable precursor may also result in forming a particulate spray or to obtain higher deposition temperatures [91].

II.1.2.4.3. Deposition Processes Involved in Spray Pyrolysis:

There are too many processes that occur either sequentially or simultaneously during film formation by spray pyrolysis for these to be modeled in a straightforward manner. These include precursor solution atomization, droplet transport and evaporation, spreading on the substrate, drying and decomposition of the precursor salt. Understanding these processes will help to improve film quality. Thin film deposition using spray pyrolysis can be divided into three main steps: atomization of the precursor solution, transportation of the resultant aerosol and decomposition of the precursor on the substrate. However, four types of processes that may occur during deposition are shown in Fig. 2.2. In process (A), the droplet splashes on the substrate, vaporizes, and leaves a dry precipitate in which decomposition occurs. In process (B), the solvent evaporates before the droplet reaches the surface and the precipitate impinges upon the surface where decomposition occurs. In process (C), the solvent vaporizes as the droplet approaches the substrate, then the solid melts and vaporizes (or sublimes) and the vapor diffuses to the substrate to undergo a heterogeneous reaction there. This is true CVD. In process (D), at the highest temperatures, the metallic compound vaporizes before it reaches the substrate and the chemical reaction takes place in the vapor phase [92].

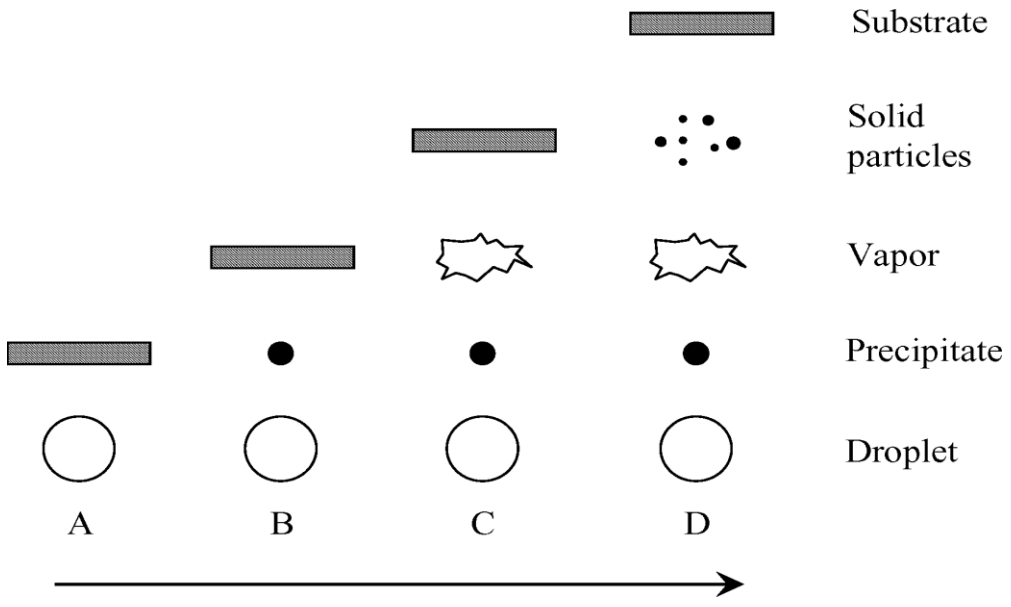

Figure 2.2: *Description of the deposition processes initiated with increasing substrate temperature or the nozzle-to-substrate distance.*

The type of spray technique used in this study is an ultrasonic spray pyrolysis. In this method, the precursor solution is atomized into the heated substrate and each atomized droplet serves as a micro-reactor which is delivered by carrier gases (air) to the reaction site and undergoes solvent evaporation, decomposition and precipitation to form the final product film.

procedure	**Material**	**Thickness or deposition rate**	**FWHM or grain size**	**Transmission (%)**	**Resistivity ρ (Ω.cm)**	**Year**
Sol-Gel [93]	ZnO ZnO :Al	250 nm	/	80-90	3,8 0,27	2003
spray pyrolysis [94]	ZnO ZnO :F	200 nm/min	250 nm	~92	10^{-1}	1998
Laser Ablation [95]	ZnO	/	$0,25^{o}$	>85	$(7\text{-}9)*10^{-3}$ $(5\text{-}8)*10^{-2}$	1994
Laser Ablation [96]	ZnO :Al	~700 nm	/	>86	5*10-4	2002
MOCVD [97]	ZnO ZnO :Ga	7 nm/min	0,28	/	10^{-2}-10^{-4}	2002
RF Magnetron [98]	ZnO :Al	150-200 nm	20-40 nm	85	$9,8*10^{-2}$	2004
RF Magnetron [99]	ZnO :Al	200 nm	/	90	$9,7*10^{-4}$	2007
DC Reactive Magnetron [100]	ZnO :Al	13,4 nm/min	$0,25^{o}$	~90	$\sim10^{-4}$	2006
Evaporation [101]	ZnO :Al	200 nm	/	>80	$4,35*10^{-3}$	1996

Table 2.2: *Typical properties of ZnO deposited with different methods*.

II.2. Characterization methods:

II.2.1. Structural Characterizations:

II.2.1.1. X-ray Diffraction (XRD):

We measured the crystallographic orientation of the layers using X-ray diffraction (XRD) spectroscopy technique. The principle, illustrated in figure (2.3), consists of focusing an X-ray beam on the sample with an angle θ and measuring the angles of diffraction of the scattered beam.

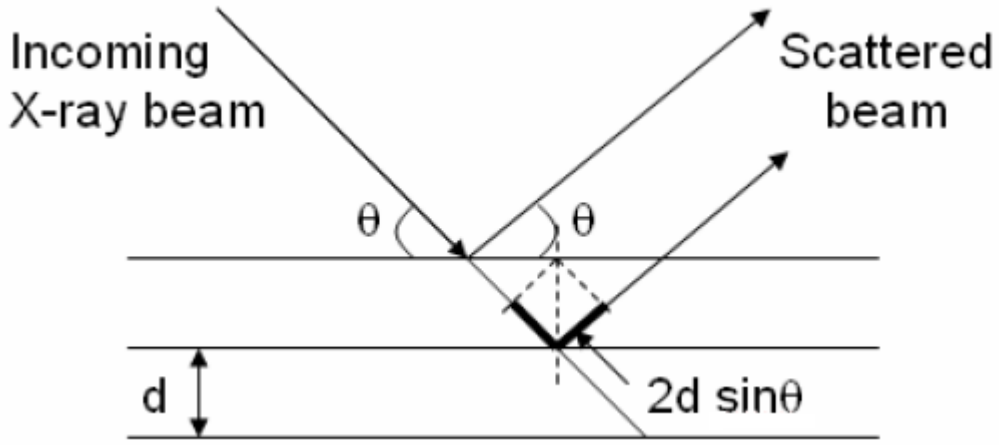

Figure 2.3 *The schematic diagram of the* θ *-2*θ *configuration for XRD measurements.*

When Bragg's law (equation 2.1) is verified, constructive interferences are formed and an intensity peak is measured.

$$2d_{hkl}\, sin\theta = n\,\lambda \qquad (2.1)$$

Where d is the distance between the lattice plans, λ the X-ray wavelength, n the diffraction order, and θ the angle defined on figure 2.3.

The X-ray spectrometer employed during this study is a D8 ADVANCE BRUKER diffractometer used in the geometry (θ -2θ scans) and equipped with a copper target (CuKα) was used to generate the incident X-rays of wavelength λ = 1.54183*A*° for the diffraction measurement.

X-ray Diffraction (XRD) is a powerful technique used to uniquely identify the crystalline phases present in materials and to measure the structural properties (strain state, grain size, epitaxy, phase composition, preferred orientation, and defect structure) of these phases [34].

II.2.1.1.1. Determination of Crystallite Size:

From the XRD pattern, the average crystallite size D could be calculated using the Scherer's formula (2-2):

$$D = k\lambda / (\Delta 2\theta)\, cos\, (\theta) \qquad (2.2)$$

Where (Δ2θ) is the full width at half maximum (FWHM as in fig.2.4) of the principal peak at 2θ (in radians), K = 0.9, is the shape factor of the average crystallite and θ is the Bragg angle.

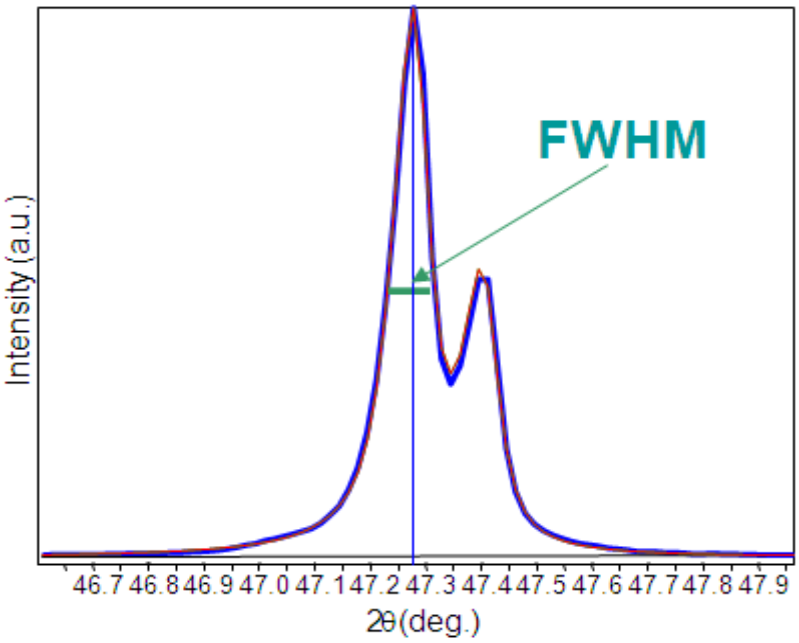

Figure 2.4: *illustration of FWHM determination.*

II.2.1.1.2. Determination of Strains:

The strains are the internal forces in the matter. If each crystallite is subjected with different strains, there is then a juxtaposition of close peaks which are superimposed. If these forces induce deformations of the unit cell (elastic strain), they will vary the interreticular distances $\boldsymbol{d_{hkl}}$ and thus shift the position of peaks. If the shift of the

peaks is measured with referring to ZnO ASTM file (figure 2.5), one can deduce the stress of the sample [102].

The recording of the spectrum of sample will enable us to determine the cell parameters. Indeed to each angle of diffraction corresponds a reticular plan (***h, k, l***) and a distance d_{hkl} in the formula of Bragg. However we know that for a cell, it exist a relation connecting the plans (***h, k, l***) and it interreticular distances d_{hkl} to intervene of cell parameters [103].

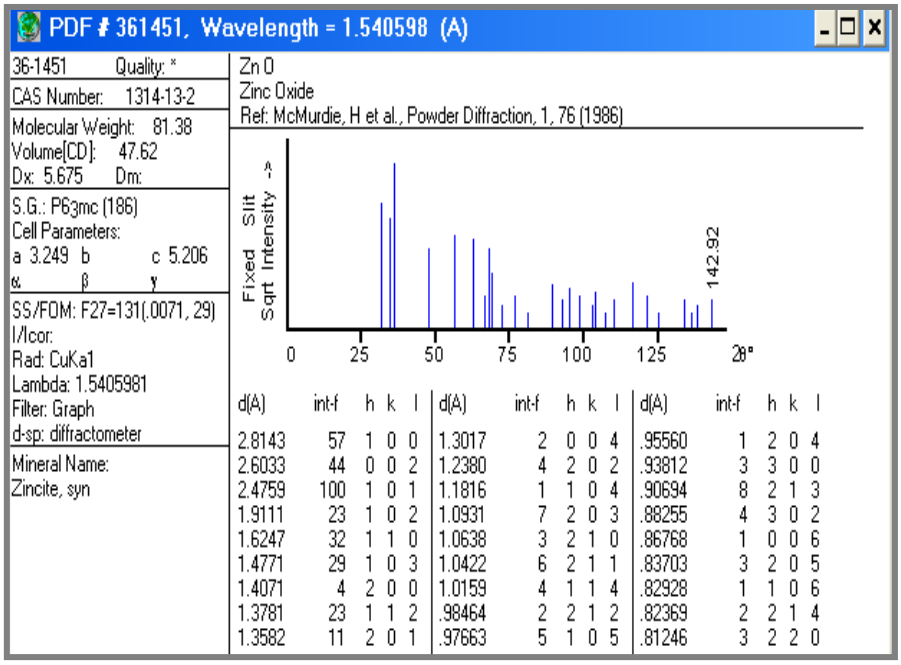

Figure 2.5: *ASTM **36-1451** file of ZnO powder.*

In our case of the hexagonal cell of ZnO, the expression is given under their form according to:

$$d_{hkl} = \frac{a}{\sqrt{\frac{4}{3}(h^2 + k^2 + hk) + l^2 \frac{a^2}{c^2}}} \qquad (2.3)$$

Where *a* and *c* are the lattice parameters,

By this formula, one can determine the parameter **c** while taking *h=k=0*, *l=2*. The measurement of the cell parameters will give an indication on the state of stresses of films by comparisons with the theoretical values $c_0 = 5.206\ A°$ of ZnO wurtzite [94].

The internal stresses can be calculated starting from the following expressions:

$$\sigma = \left[2c_{13} \frac{(c_{11} + c_{12}) c_{33}^{film}}{c_{13}} \right] e_{zz} \quad (2.4)$$

With: $c_{33}^{film} = \frac{0.99 c_{33}^{cristal}}{(1-e_{zz})^4}$ and: $e_{zz} = \frac{c_0 - c}{c}$

For C_{11}, C_{12}, C_{13} and C_{33} appearing in these formulas, we have used respectively values 209,7, 121,1, 105,1 and 210,9 GPa [54].

II.2.1.2. Scanning electron microscopy (SEM):

The electronic microscope is based on the analysis of the interactions electron / matter during the bombardment of the sample by a beam of electrons.

The basic steps involved in all SEM are the following: A stream of electrons is formed in high vacuum (by electron guns). This stream is accelerated towards the specimen (with a positive electrical potential) while is focused using metal apertures and electromagnetic lenses. In the final lens, the SEM contains extra sets of coils that allow it to deflect the electron beam back and forth across the sample.

The interaction between the electrons beam and the sample cause the emission of secondary electrons, Auger electrons, backscattered electrons, visible light and X-rays.

The most common imaging mode collects low-energy (<50 eV) secondary electrons that are ejected from the k-orbital of the specimen atoms by inelastic scattering interactions with beam electrons. Due to their low energy, these electrons originate within a few nanometers from the sample surface.

A JSM-6390LV JEOL microscope is used to visualize the surface of the ZnO films. We use the same equipment in EDX mode in order to perform chemical analysis.

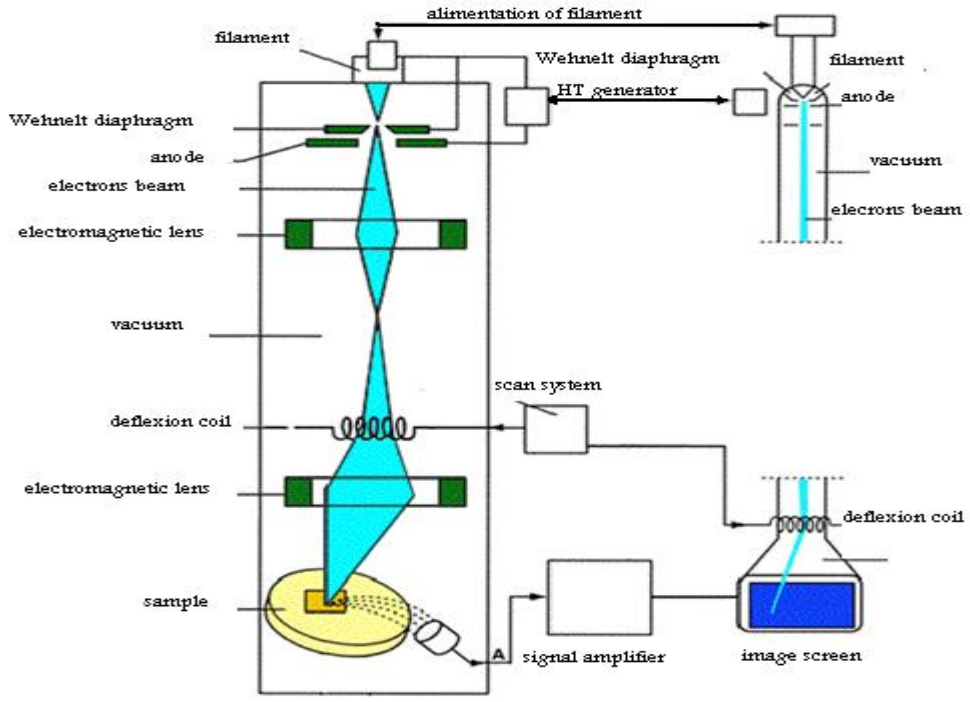

Figure 2.6: *schematic representation of scanning electronic microscopy.*

II.2.1.3. Energy Dispersive X-ray analysis (EDX):

EDX is an analytical technique which utilizes x-rays that are emitted from the specimen when bombarded by the electron beam to identify and quantify the elemental composition of the specimen. To explain further, when the sample is bombarded by the electrons beam of the SEM, electrons are ejected from the atoms on the specimens surface. A resulting electron vacancy is filled by an electron from a higher shell, and an x-ray is emitted to balance the energy difference between the two electrons. The EDX x-ray detector measures the number of emitted x-rays versus their energy. The energy of the x-ray is characteristic of the element from which the x-ray was emitted [104].

The energy dispersive x-ray analysis system is usually attached to a scanning electron microscope system (SEM).

II.2.2. Optical characterization:

The ratio of the transmitted light intensity I to the incident light intensity I_o, when light is passed through an absorbing film, is given by Beer-Lambert relation:

$$I = I_O \, exp\,(-\alpha d) \qquad (2.5)$$

Where α is the absorption coefficient and d the thickness of the film.

The transmittance T (quantity of the transmitted light) can be directly measured, where: $T(\%) = I/I_o . (100)$

And thus, for a film of known thickness, the absorption coefficient can be calculated from the transmission data.

$$\alpha = \frac{1}{d\ ln}\left(\frac{100}{T\ (\%)}\right) \qquad (2.6)$$

The absorption coefficient α is related to the extinction coefficient k by the equation:

$$\alpha = \frac{4\pi k}{\lambda} \qquad (2.7)$$

Where λ is the wavelength of the light.

We measured the sample transmittance spectra with dual beam UV-VIS-NIR scanning spectrophotometer of type SHIMADZU UV-3101 PC, its operation principle is represented in (figure 2.7)

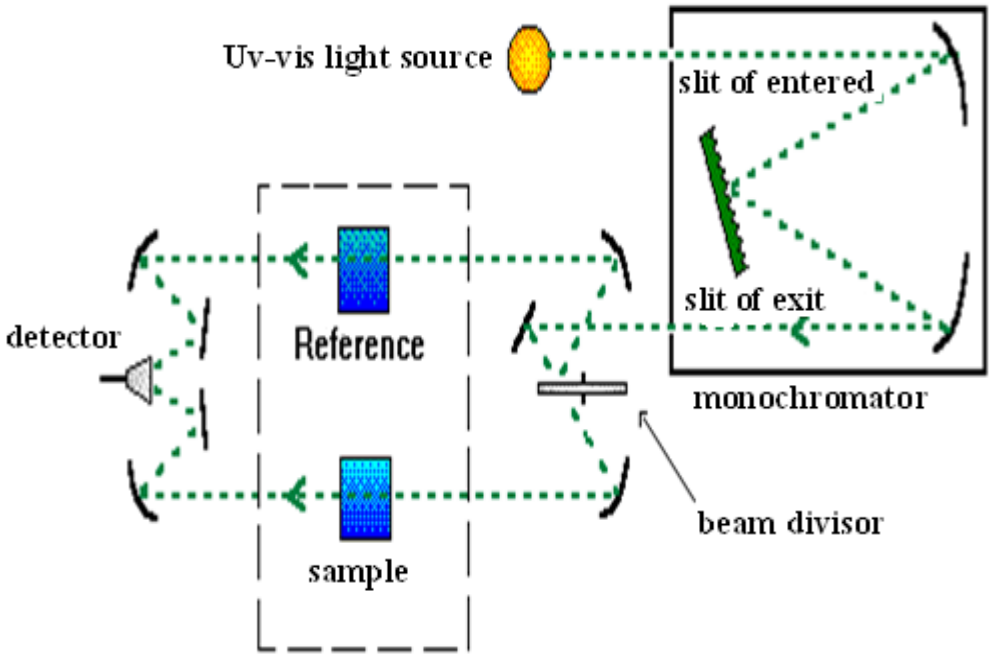

Figure 2.7: *schematic representation of spectrophotometer*.

II.2.2.1. Optical gap determination:

The fundamental absorption is related to the band-to-band transitions in a poly-crystalline semiconductor, i.e., to the excitation of an electron from the valence band to the conduction band. Therefore, the fundamental absorption can be used to determine the energy gap of the semiconductor.

The absorption coefficient is related to the optical bandgap via Tauc's relation [105]:

$$(\alpha h\nu)^2 = A\,(h\nu - Eg) \quad (2.8)$$

Where h is Planck's constant, ν is the photon frequency; A is constant and Eg is the band gap of the film.

If we plot $(\alpha h\nu)^2$ in function of photon energy E= hν (with hν (eV) = hc / λ = 12400 / λ(A°)) and with prolonging the linear part of $(\alpha h\nu)^2$ to x-coordinate axis (i.e., $(\alpha h\nu)^2 = 0$), we obtain Eg value (figure 2.8).

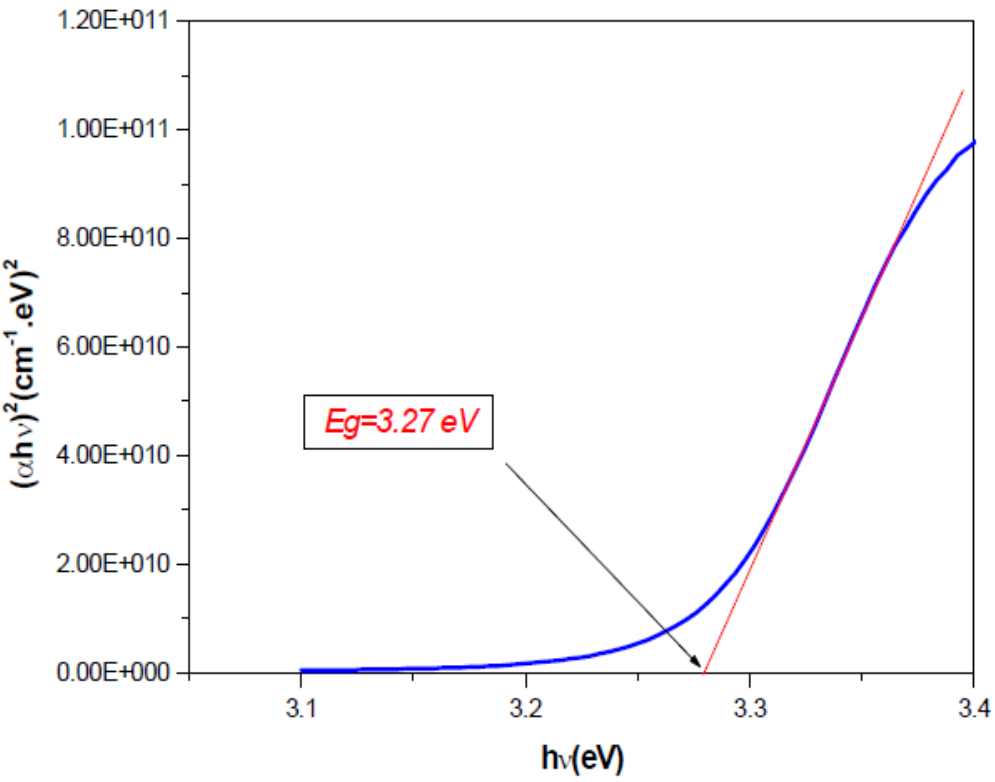

Figure 2.8: *illustration of band gap determination*.

II.2.2.2. Localized states and Urbach tails:

The empirical parameter E_{00}, often referred to as the "*Urbach tails*" has the dimensions of energy and is frequently used to determine the film quality (measures the degree of disorder in amorphous semiconductors) [106]. Eu is usually used to describe the width of the localized states in the bandgap (but not their positions). Pankove has shown that the value of Eu is related to the impurity concentration [107]. However, Redfield has shown that all defects (point, line, and planar defects) lead to local electric fields that cause band tailing. Thus, the Urbach energy can be considered a parameter that includes all possible defects [108].

In this work, the Urbach tail is used as a parameter for assessing the amount of disorder in ZnO films.

$$\alpha = \alpha_0 exp\,(h\nu / Eoo) \qquad (2.9)$$

By drawing $ln(\alpha)$ versus $h\nu$ we can determine *Eu* value as the reciprocal of the linear part slope (figure 2.9):

$$ln(\alpha) = ln(\alpha_0) + (h\nu/Eoo) \qquad (2.10)$$

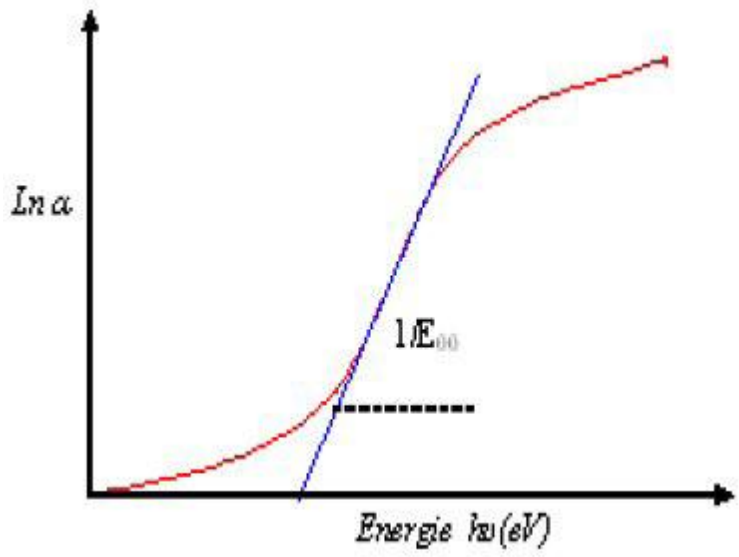

Figure 2.9: *illustration of Urbach energy determination.*

II.2.3. Electrical Characterization:

II.2.3.1. Two point's technique:

The conductivity measurements of solution flow rate series were carried out using two points method (coplanar) (figure 2-9), where we realized two electrical contacts of gold (electrodes), were separated by 5mm of distance, and were deposited by an Edward sputter coater S150B.

A variable tension V applied between the electrodes of the sample thus creating a current I measured using a KEITHELY pico-amperemeter which can measure weak currents. The slope of the characteristic current-voltage is the value of resistance R, from Ohm's law:

$$R = V / I \qquad (2.11)$$

This law represents a linear variation between the current and the tension (ohmic contact). The calculation of electrical conductivity σ depends on electrical resistance R, as well as geometrical parameters (fig.2.10): the distance between electrodes L, the thickness d, and the width of film w as follows:

$$\sigma = (L / w.d)\ (1/R) \qquad (2.12)$$

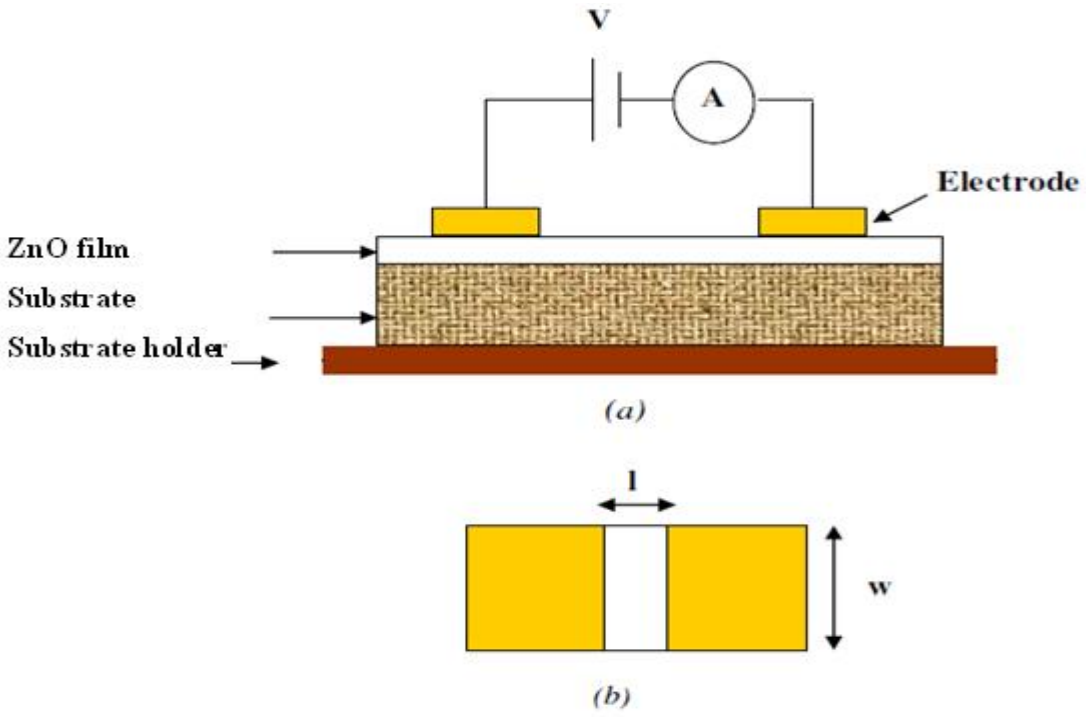

Figure 2.10: *(a) electrical scheme of system; (b) the dimensions of the film*

II.2.3.2. Van der Pauw technique :

The Van der Pauw technique, due to its convenience, is widely used in the semi-conductor industry to determine the resistivity of uniform samples. [109] As originally devised by Van der Pauw, one uses an arbitrarily shape, thin-plate sample containing four very small ohmic contacts placed on the periphery, preferably in the corners, of the plate. A schematic of a rectangular Van der Pauw configuration is shown in Figure 2.11.

The objective of the resistivity measurement is to determine the sheet resistance *R*S. Van der Pauw demonstrated that there are actually two characteristic resistances R_A and R_B, associated with the corresponding terminals shown in Figure 2.10 *R*A and *R*B are related to the sheet resistance *R*S through the Van der Pauw equation:

$$exp\left(-\frac{\pi R_A}{R_S}\right) + exp\left(-\frac{\pi R_B}{R_S}\right) = 1 \qquad (2.13)$$

This can be solved numerically for R_S.

The bulk electrical resistivity ρ can be calculated using:

$$\rho = (\pi . d)/0.69 \ \ (R_A + R_B)/2 \ f(R_A/R_B) \qquad (2.14)$$

Where d is the thickness of the film, $f(R_A/R_B)$ is a correction factor between 0 and 1 related to the ratio R_A/R_B.

The Van der Pauw measurements were carried out by PHILIPS multi-meter which can measure resistance until $10^6\Omega$. The contacts were deposited by the same sputter which used in two points technique.

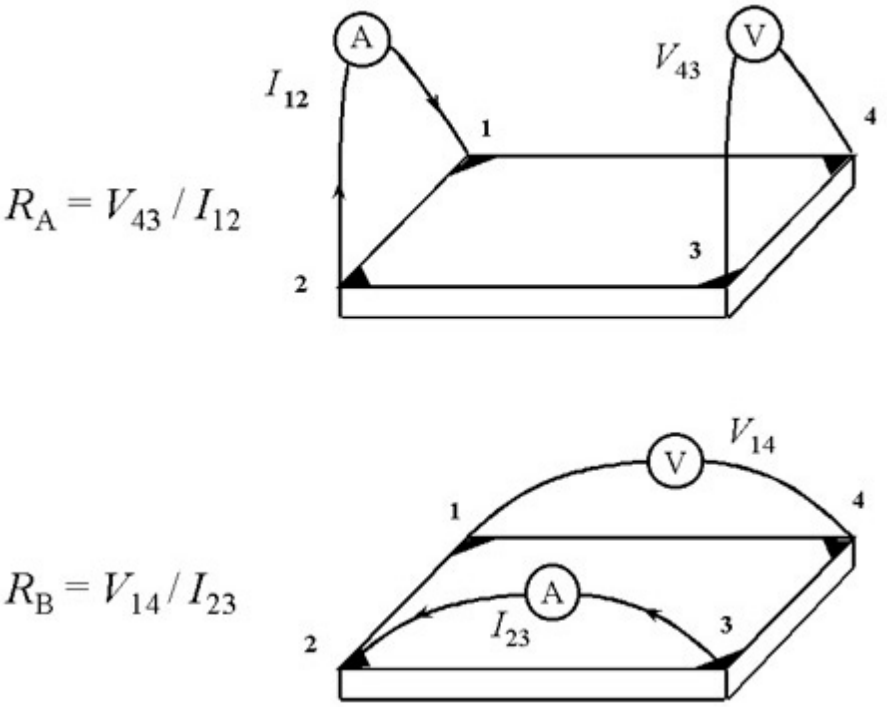

Figure 2.11: *Schematic of a Van der Pauw configuration used in the determination of the two characteristic resistances R_A and R_B.*

CHAPITRE III

ELABORATION AND CHARACTERIZATION OF ZnO THIN FILMS BY ULTRASONIC SPRAY PYROLYSIS

III.1.Elaboration of ZnO Thin Films:

Introduction:

In this chapter, the experimental procedures for developing the novel spray pyrolysis system and its application in processing of ZnO thin films based on optimization of processing parameters are explained in detail. Through designed set of experiments, the range of initial spray conditions which relate to the system such as solution flow rate, nozzle-to-substrate distance, and carrier gas (air) pressure, over which the ZnO film could be reproducibly deposited on glass substrate was determined. During each step, all these deposition parameters were kept constant except for the parameter that is going to be investigated. It was verified that some deposition parameters have different effects on thin film proprieties. Physical and chemical properties during spray pyrolysis are presented and compared with the data available in the literature. Based on these results, optimum parameters were concluded. ZnO thin films were successfully deposited on glass substrate. The thin film crystallinity, composition, and microstructure, optical transparency and electrical conductivity measurement were characterized by XRD, EDS, SEM, UV-VIS spectrophotometer, two points and four points respectively.

III.1.1. Development of a Novel Spray Pyrolysis System:

III.1.1.1. Ultrasonic Spray Pyrolysis Setup:

Fig.3.1 shows the schematic and of the ultrasonic spray pyrolysis setup that has been developed in our laboratory. Similar to other spray systems it consists mainly of:

Ultrasonic generator (SONICS): it contains different electric devices which work to generate ultrasonic waves with constant frequency 40 KHz and variable amplitude at the atomizer level.

Atomizer: It is fabricated from titanium alloy Ti-6Al-4V as piezoelectric transducer. It makes it possible to transform the solution into a jet of very fine droplets of 60 µm in average diameter, placed on an adjustable holder in order to control the distance nozzle-substrate.

A compressor (*JUN- AIR*, 6-S type): It is the novelty part of our spray pyrolysis system which allows compressing the carrier gas (the air). By suitable way it is connected with the nozzle for guiding generated droplets with considerable velocity toward the heated substrate.

Substrate holder: a hotplate heats by an electric resistance where the temperature can be controlled and measured by a thermocouple.

Solution flow rate regulator: it is a small reserve of solution source which supplies by gravity an ultrasonic spray pyrolysis with a low solution flow rate which can be controlled by changing the difference of solution level between reserve and atomizer.

Electrical motor: works to move the atomizer back and forth to obtain the same proprieties of aligned substrates.

Other elements: are materials used: syringe (to keep volume level in the solution reserve constant), to measure deposition time (chronometer), other laboratory instrument (test tube, burette…) and electronics circuits and transformers.

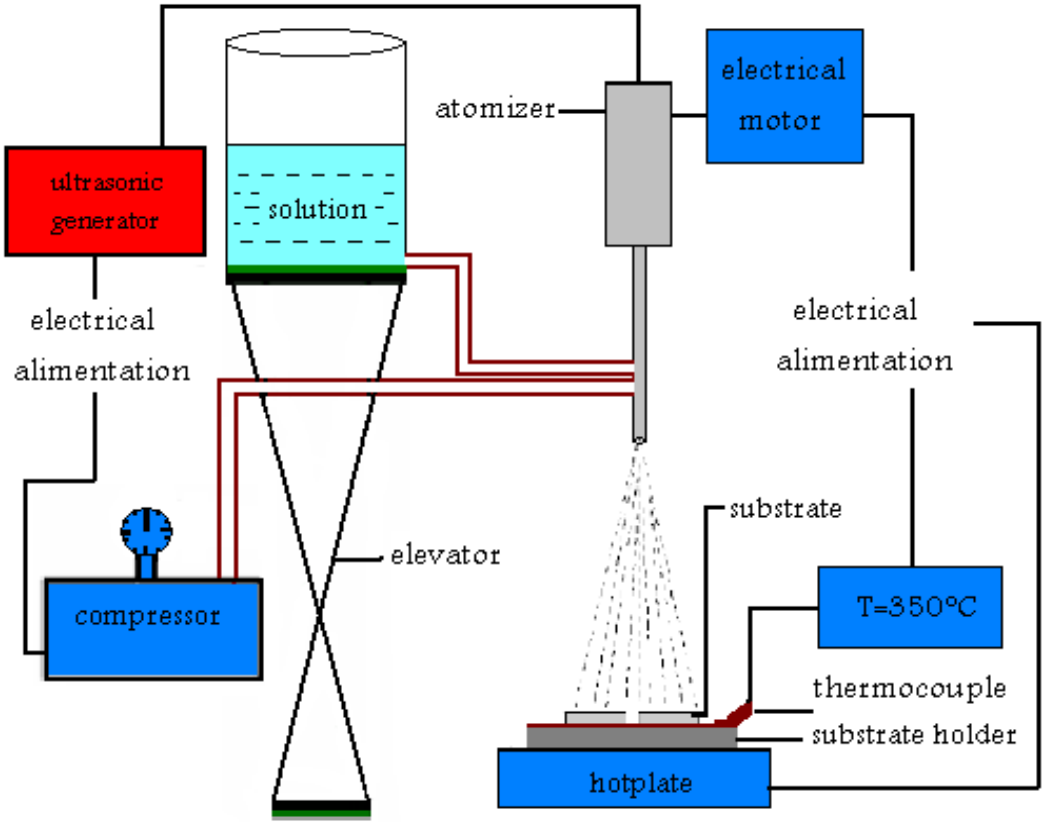

Fig.3.1: *Schematic of the ultrasonic spray pyrolysis setup.*

III.1.1.2. Experimental Procedure:

Before thin films deposition procedure, we started with calibration and sometimes operational tests of the deposition system. The goal of this preliminary work is the adjustment of our parameters system in order to make the deposition procedure reproducible.

For adjusting the solution flow rate and make it controllable, several attempts carried out until we arrived to use the gravitational energy by changing the vertical distance between the highest level (solution level in the reserve) and the lowest level (atomizer).

The ultrasonic atomizer which is connected with the ultrasonic generator work to fractionate the chemical solution to micro droplets when it passing through the piezoelectric transducer, these droplets falls on the heated substrate but some of them lose randomly and do not reach the substrate. In order to avoid this lost amount of solution

we added air pressure at the atomizer inlet which allows guiding the generated droplets toward the substrate. This additional part makes the deposited amount constant at every time.

When the droplets reach the heated substrate, the chemical reaction starts under elevating temperature effect to form the thin film. The temperature measurement carried out by Fer-Constantan thermocouple (J type). This thermocouple is fixed on steel holder which putted on a hotplate (electrical resistance 1000 watts). The temperature adjustment is realized by using a numerical thermo-regulator (EC 3-133; EVRY CONTROL). We selected the holder from steel mater due to its good saving of heat.

III.1.2. Experimentation:

III.1.2.1. Preparation of Substrates:

The substrates used are glass blades of square surface 1.5 X 1.5 cm^2 and 1mm of thickness, which cut out by diamond pen and cleaning according to the following steps:

- 5min in distilled water.
- 10min in acetone.
- 5min in distilled water.
- 10min in alcohol (ethanol).
- Drying in furnace.

The clean of substrates is an important procedure to avoid any contamination which effect electrical and optical proprieties.

We choose glass blades for two reasons:

- It makes it possible to carry out a good optical characterization of films.

-After the deposition the samples (substrate + film) will undergo a cooling from the higher temperature of deposition at 350° C until the ambient temperature (~25°C) which causes shrinkage of two materials which constitute the sample. In this case, they have very close coefficients dilation, then a minimization of the stresses.

III.1.2.2 Preparation of Solutions:

The precursors (for example, nitrates, acetates or chlorides of metal) are dissolved in distilled water or alcohol (solvent) to obtain the desired molar concentration. In our work we used Zinc chloride ***($ZnCl_2$)*** as precursor solution, its molar weight M=136, 29 ($g.mole^{-1}$).

These precursor solutions were dissolved in distilled water at constant molar concentration **C**= 0.1 $mole.L^{-1}$ during all experiments by using instruments of laboratory of chemistry at university of Biskra such as test tubes, flacons, burettes,… and *Princeton SA2004B* balance with precision of 10^{-4}g.

III.1.2.3 Deposition of Thin Films:

In order to be able to analyze the trend of changing the structural, optical and electrical proprieties with variation of one parameter, other deposition parameters should be fixed during the experiment and their effects need to be assumed negligible during the investigations.

After the preparation of solution (distilled water + precursor) and filling the solution reserve until specified level which is kept constant during the deposition time. The generated droplets start reacting in the spacing above heated substrate at elevated temperture 250 and 350°C. The chemical reaction occurs as follows:

$$ZnCl_{2(solid)} + H_2O_{(liquid)} \rightarrow ZnO_{(solid)} + 2HCl_{(gas)}.$$

To avoid the thermal crash and the deformation or the breaking of glass substrates we maintain the sample after enough time until the temperature reaches the ambient temperature.

In both D and B series the amplitude of the ultrasonic generator was kept constant at 100%, but in S series we adjust it at 65% to avoid the damage of our generator.

The spray conditions are summarized down in Table 3.1.

Sample	Temperature (C°)	Air pressure (bar)	Deposition rate ($ml.min^{-1}$)	Distance bec-substrate (cm)	Depositition time (sec)
D0	**250**	**0.05**	**0.31**	**7.5**	**575**
D1			**0.34**		**530**
D2			**0.48**		**372**
D3			**0.57**		**315**
D4			**0.91**		**197**
D5			**1.4**		**129**
D6			**2**		**90**
D7			**2.85**		**63**
B1	**350**	**0.15**	**0.48**	**5**	**115**
B2				**8**	
B3				**11**	
B4				**14**	
B5				**15.5**	
B6				**17**	
B7				**20**	
S1	**350**	**0**	**0.48**	**15.5**	**115**
S2		**0.05**			
S3		**0.1**			
S4		**0.15**			
S5		**0.2**			
S6		**0.25**			
S7		**0.3**			
S8		**0.35**			

Table.3.1: *Table of spray conditions for all optimization experiments.*

III.2. Results and Discussion:

Introduction:

In this part we show the characterization results and their interpretations in order to determine the optimum conditions which give best microstructure, composition and optoelectronics proprieties for each parameter effect. The parameters which we studied their effects on ZnO thin film proprieties are: precursors, solution flow rate, nozzle-to-substrate distance and air pressure.

III.2.1. Effect of Solution Flow Rate:

Through this experiment we changed the solution flow rate from the minimum possible value which corresponds 1cm in the difference of solution level for the flow rate solution 0.31 ml/min to the maximum possible value which corresponds 25cm in the difference of solution level for the flow rate solution 2.85 ml/min when the chemical reaction didn't take place because the thermal energy doesn't be enough for this amount of solution therefore the solvent (water) vaporizes and zinc chloride deposits on the substrate.

The effect of solution flow rate on the chemical composition is emerged in Fig.3.2. The stoechiometry analysis of the material is difficult because it requires a special treatment, also the substrates used (SiO_2) can be a source of error in the estimation of oxygen rate in films.

These EDS analysis shows the increasing of oxygen atoms against zinc atoms in the sample D1 and a rapprochement in the number of these atoms in the sample D5. The presence of silicon atoms with considerable amount demonstrates that the rate of oxygen atoms come from the film and the glass substrate, therefore the number of oxygen atoms could be less than zinc atoms in our films, especially in the sample D5 than D1.

D5 surface also contains traces of chlorine are coming from the molecules which do not reach the reaction of pyrolysis due to the high flow rate ($1.4ml.min^{-1}$) and little amount of calcium atoms maybe come from the glass substrate.

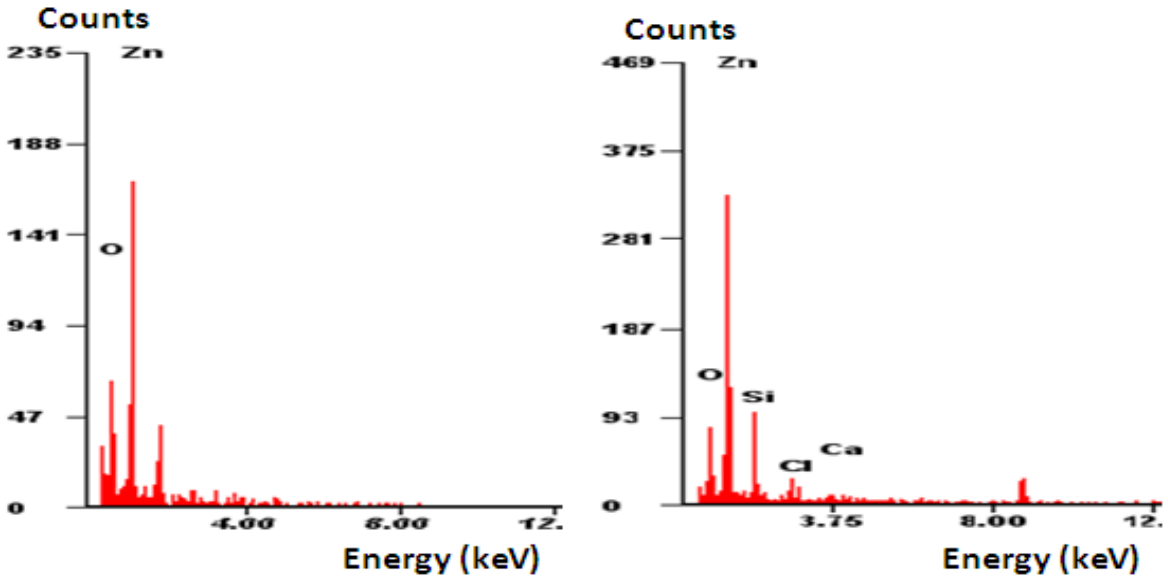

Element	Wt %	At %
Oxygen	26.00	58.94
Zinc	74.00	41.06
Silicon	/	/

(D1)

Element	Wt %	At %
Oxygen	14.77	35.55
Zinc	62.46	36.78
Silicon	12.59	17.25
Chlorine	5.17	5.61
Calcium	5.07	4.81

(D5)

Figure.3.2: *EDS spectra of samples deposited at flow rates 0.34ml/min (D1) and 1.4ml/min(D5).*

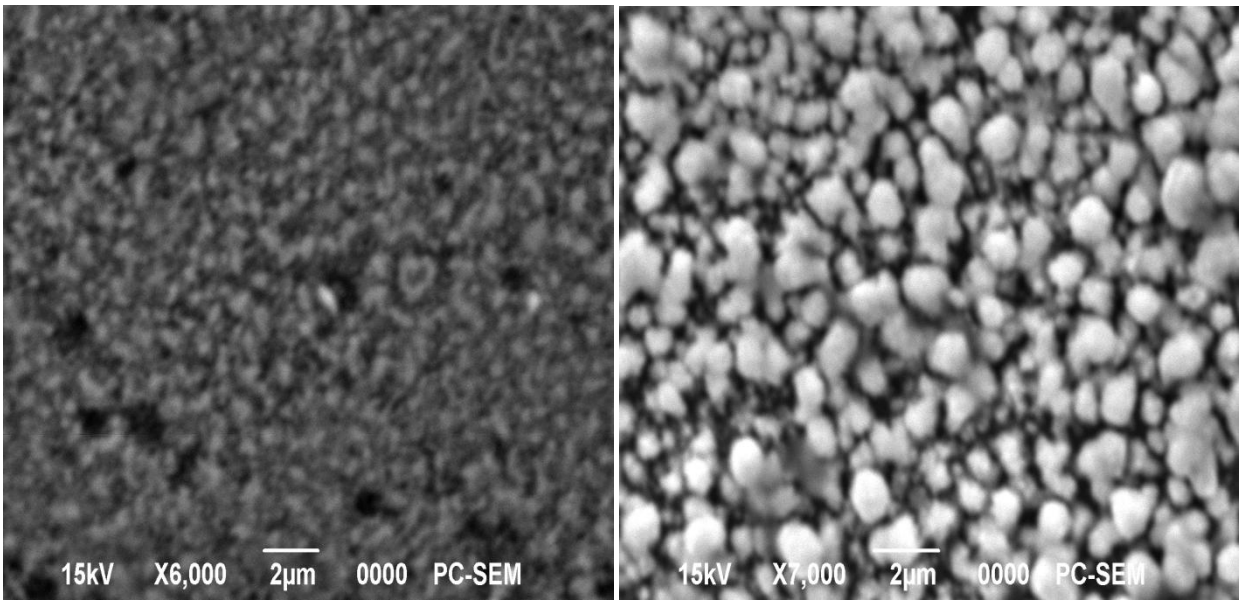

(D1) (D5)

Figure.3.3: *SEM micrographs of ZnO films sprayed at flow rate 0.34ml/min (D1) and 1.4ml/min (D5).*

Scanning electron microscopy (SEM) pictures of these films are depicted in Figure 3.3. It is observed that the surface morphology of both samples are uniforme.

Figure 3.4 represents the XRD patterns of the ZnO thin films. As illustrated, for all deposition rates the films have the wurtzite polycrystalline structure of ZnO with preferred orientation along (0 0 2) at 2θ =34.56° (JCPDS Card N°. 36-1451). This preferred orientation means that the `c` crystallographic axis is perpendicular at the substrate, which means orthogonal growth direction, this plan requires the lowest energy of formation [111]. This preferred orientation was observed by other others [112,113].

We observe appearing of other secondary peaks for higher deposition rates at 2θ= 36.3°, 47.6° and 62.75° for these orientations (101), (102) and (103) respectively.

The strongest peak along (0 0 2) is observed at the deposition rate 1.4ml/min and the other peaks are so weak; this is attributed to the increasing in the film thickness at high deposition rates.

From these XRD spectra we estimate FWHM (full width at half maximum) and stress values which are presented in Figure 3.5. We observe that FWHM of the principal peak (002) decreases from 0.198° to 0.192° with increasing the deposition rates until 0.48 ml/min, therefore the mean grain size increases from 42.3 to 43.6nm. After that it increases to 0,208° for films deposited at deposition rate 2 ml/min, so the mean grain size decreases to 40.2nm for the same solution flow rates respectively.

The stress value changes exhibit a concurrence with FWHM changes; the minimum stress value corresponds with the minimum FWHM for the sample D2 at deposition rate 0.48ml/min which means the best structure.

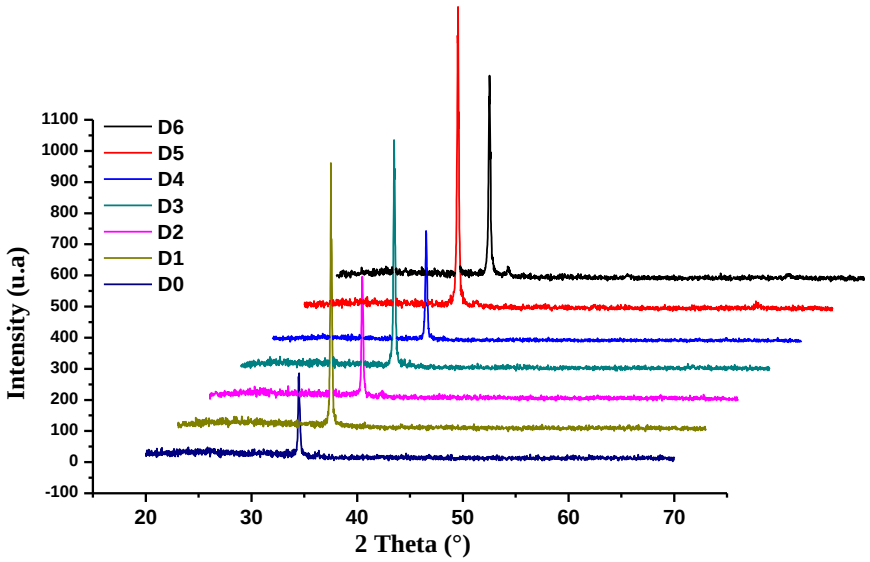

Figure.3.4: *XRD spectra of films deposited at different solution flow rates.*

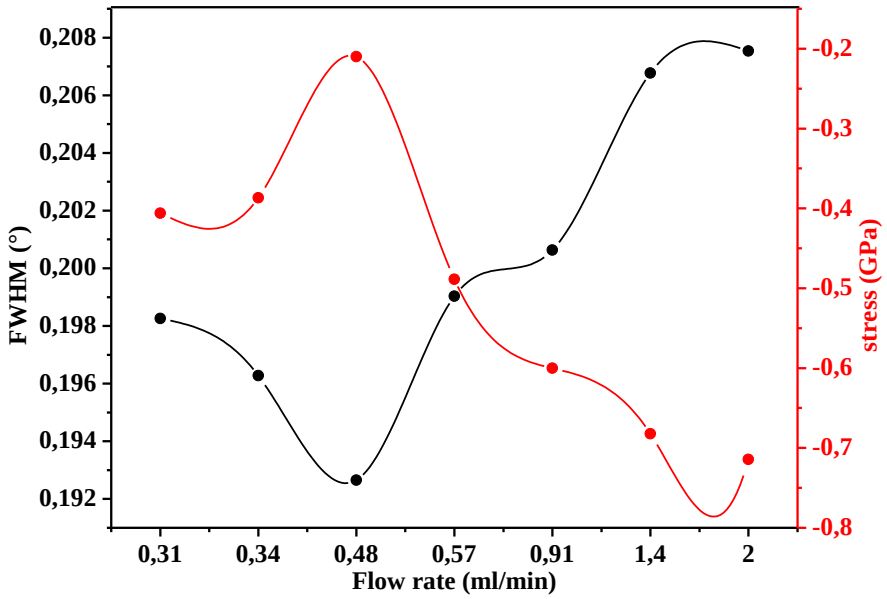

Figure.3.5: *FWHM and stress variations vs. solution flow rates.*

The figure.3.6 shows the measured transmittance spectra as a function of the wavelength in the range 290-800 nm for films deposited at various solution flow rates. We observe that the transmittance in the visible range increases from 52% for the low solution flow rate 0.3 ml/min to values ~60% for 0.48 ml/min due to the improvement in cristallinity. Then it decreases particularly with increasing solution flow rate until values lower than 20% for the high solution flow rate (2ml/min). This decreasing in the

transmittance is attributed to the increasing in the deposition rate which increases the film thickness and decreases the cristallinity, the homogeneity and the stoechiometry.

Actually in the area of strong transmittance, we could obtain interference fringes. These fringes are due to the multiple reflections on the two interfaces of film. The absence of these interference fringes in our samples is due to the roughness of the free face. This roughness causes the diffusion of light instead of the reflection on the interface. The roughness of surface is often a characteristic of films obtained by spray, due to the growth mechanism of this technique.

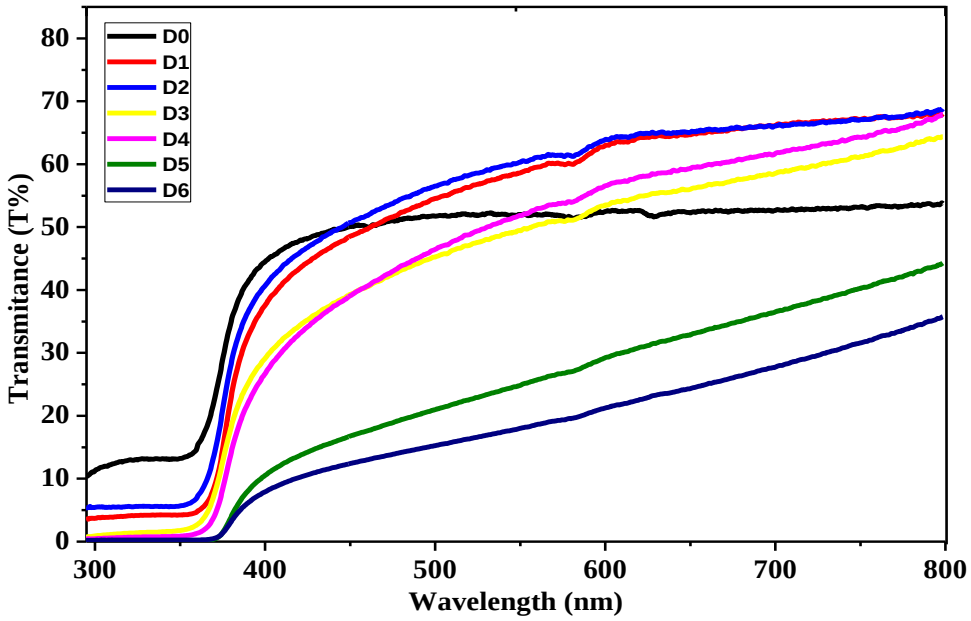

Figure.3.6: *Optical transmittance spectra for films deposited at different flow rates.*

The figure.3.7 shows the variation of the energy gap and Urbach energy for different solution flow rates. The values of energy gap (3.22-3.25 eV) are comparable with those given by other authors [114]. We note a broadening of the gap with the rise in the solution flow rate. With increasing the deposition rate, the thickness of the film deposited increases, also the number of zinc atoms increases versus the number of oxygen atoms. So according to" Burstein-Moss ", this broadening is related to the increase in the number of free carriers (electrons) of n-type ZnO thin films.

Urbach energy decreases with increasing the deposition rate from 0.23 to 0.15eV. The disorder is characterized by the width of the localized states in the band gap. The

optical gap is the energy gap between the two bands of band tail. Consequently, a reduction of disorder is accompanied by a widening by the optical gap.

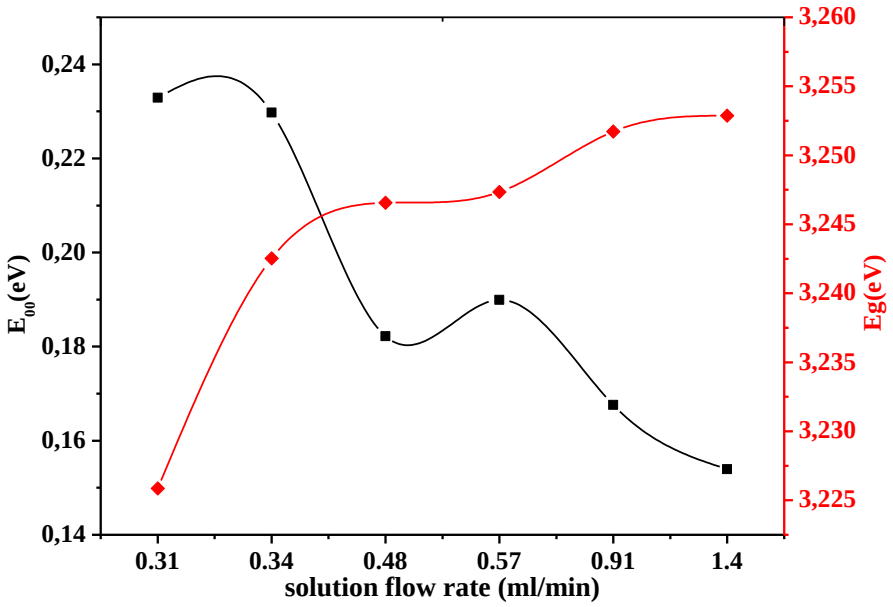

Figure.3.7. *Variation of gap energy (E_g) and Urbach energy (E_{00}) for different solution flow rates.*

From the technique of two points, we deduced the changes of the electrical conductivity of films deposited at different solution flow rates. These electrical conductivity values are presented in Figure.3.8. Generally the conductivity increases by increasing the deposition rate due to the increasing in film thickness and the non-stoechiometry which causes the number of free carriers. These values are comparable with those found by Garnier et al [116]. For both films deposited at deposition rates 0.91 and 2ml/min the film thickness is less than which is before it.

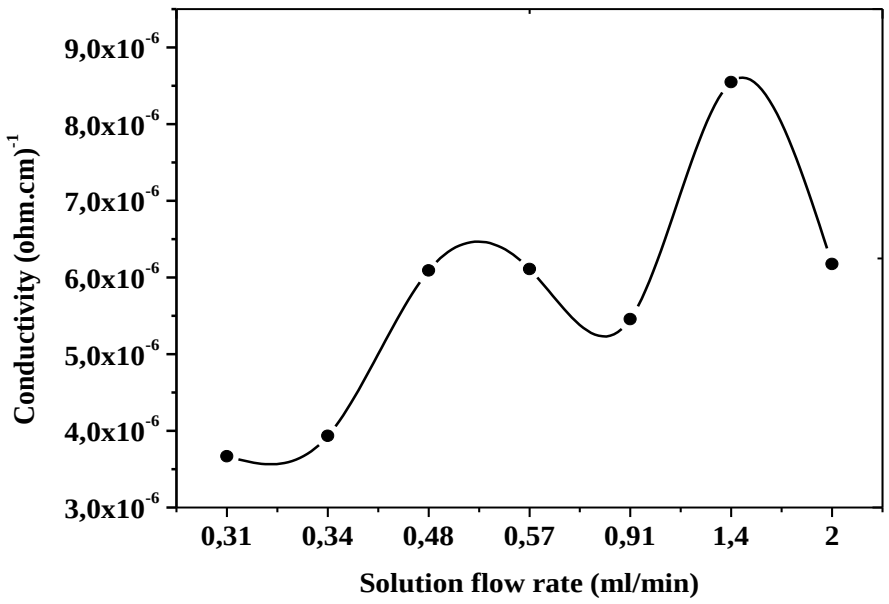

Figure.3.8: *Variation of conductivity for different solution flow rates.*

Discussion:

Solution flow rate is critical factor influencing the mechanism of film growth as it determines the time available for a droplet to reach the surface and react before a second drop strikes the same area on the surface [110]. With the increase in solution flow rate the effect of the temperature decreases, therefore the effect of solution flow rate is similar of the effect of the substrate temperature as we shown in Fig.2.2. The process at low solution flow rates 0.31 and 0.34ml/min is similar to process (D), the process at solution flow rates around 0.48 ml/min is similar to process (C), the process at higher flow rates is similar to process (B) and (A).

We indicated that the film thickness increases with the increase in solution flow rate; this could be attributed to the decrease in the ultrasonic atomizer capability when the amount of solution is increasing, therefore the air pressure can't spread the droplets as in lower solution flow rates, then the density of droplets increases.

From the results of this study at the effect of solution flow rate we can deuce that the optimum solution flow rate which gives best structural, optical and electrical properties is approximately 0.48ml/min. And we will adjust the deposition rate at this value in the next experiments.

III.2.2. Effect of Nozzle-to-Substrate Distance:

Table 3.1 shows the spray conditions for the study of the effect of nozzle-to-substrate distance on ZnO thin films proprieties. The range of nozzle-to-substrate distance for formation of a reasonable coating has to be 5-20 cm. However, this range is specific for our spray system setup and could be different in other types of spray systems.

The effect of nozzle-to-substrate distance on the structural proprieties is presented in Fig.3.9. All samples shows the wurtzite polycrystalline structure of ZnO with preferred orientation along (0 0 2) at 2θ = 34.5°.

It's obvious that with decreasing in nozzle-to-substrate distance the intensity of the principal peak increases, also other secondary peaks appear for distances 8cm and 5cm at 2θ= 31.85°, 36.25°, 47.56°, 56,52°, 62,85°,67.98° and 72.56° for these orientations (100), (101), (102), (110), (103), (112) and (004) respectively. These changes are attributed to the increasing in film thickness with decreasing nozzle-to-substrate distances.

The FWHM changes at different nozzle-to-substrate distances are presented in Fig.3.10. We can see that the distance 15.5cm gives the best structure which has the minimum FWHM value 0.154°.

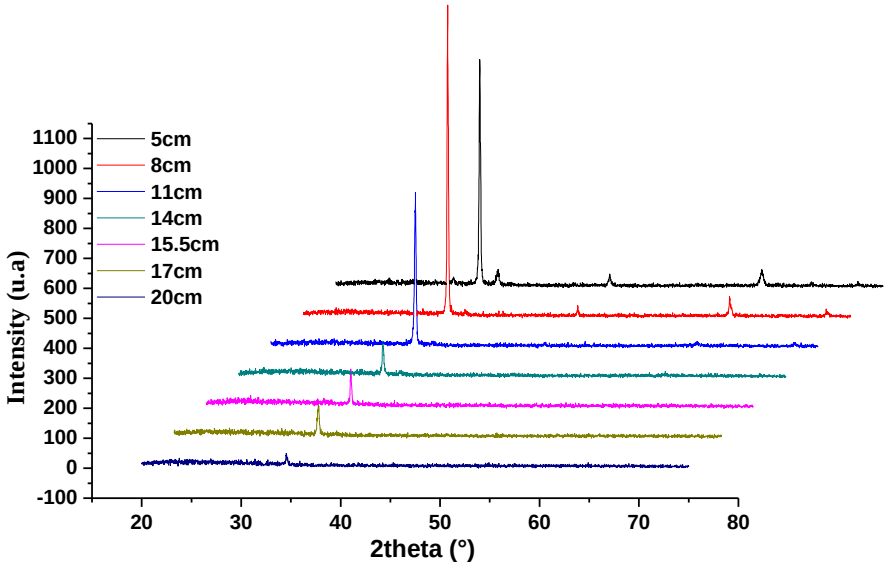

Figure.3.9: *XRD spectra of films deposited at different distance nozzle-substrate.*

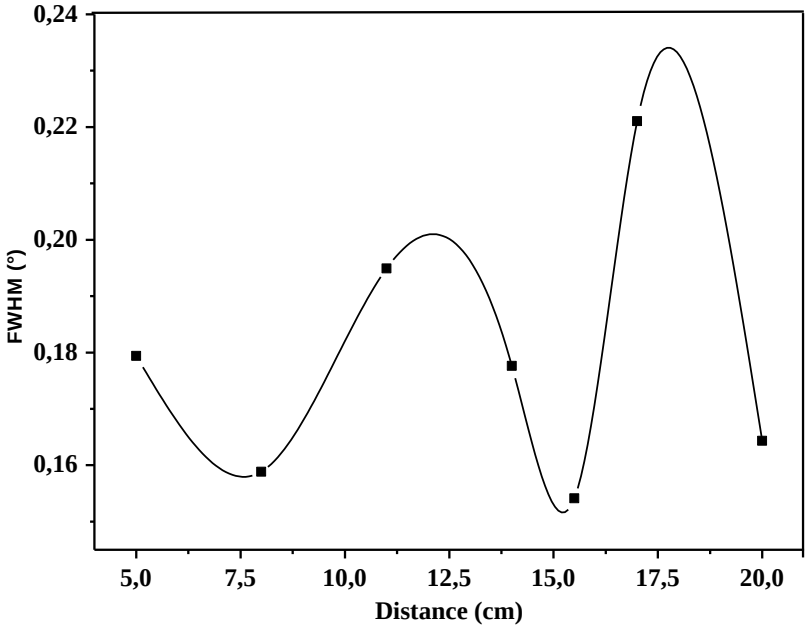

Figure.3.10: *FWHM variation for different nozzle-substrat distances.*

The figure.3.11 shows the measured transmittance spectra versus the wavelength in the range 300-800 nm for films deposited at different nozzle-substrate distances. Approximately, we observe that the optical transmittance in the visible region increases from T≈10% to T>80% with increasing the nozzle-substrate distances. This increase is due to the decreasing in the film thickness. These values are comparable with other results in literature [115].

The absence of the interference fringes in these transmittance spectra is due to the roughness of the film surfaces.

Figure 3.12 represents the changes of energy gap and Urbach energy as function of nozzle-to-substrate distances. We can observe that the energy gap has the higher values E_g= 3.225-3.19 eV for nozzle-to-substrate distances shorter than 15cm, and the lower values E_g= 3.13-3.17 eV for distances greater than 15cm. This could be attributed to the decrease in the film thickness and the increase in the number of oxygen atoms against zinc atoms with the increase in nozzle-to-substrate distances.

Urbach energy increases with increasing the nozzle-to-substrate distance from 0.11 to 0.28eV, the increasing in Urbach energy could be attributed to the shrinkage in the energy gap.

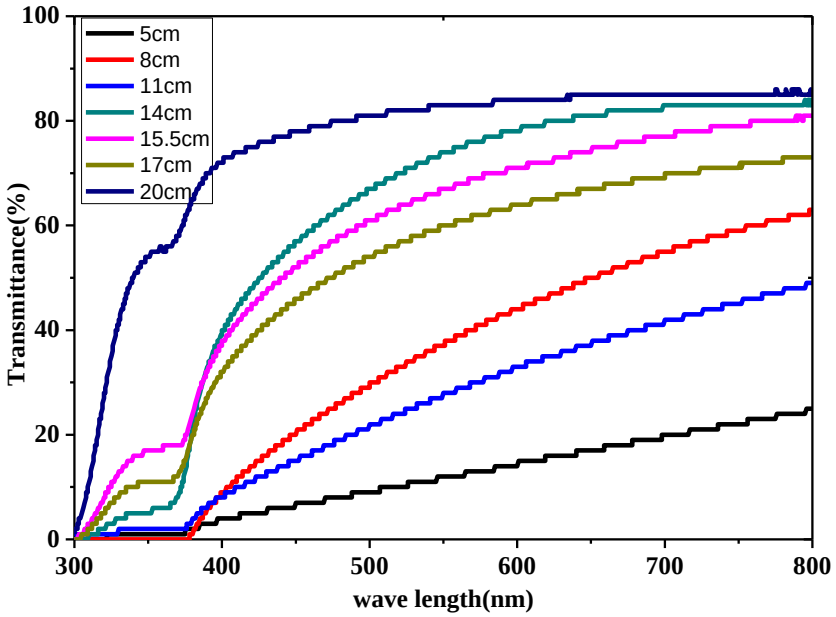

Figure.3.11: *Optical transmittance spectra for films deposited at different nozzle-substrate distances.*

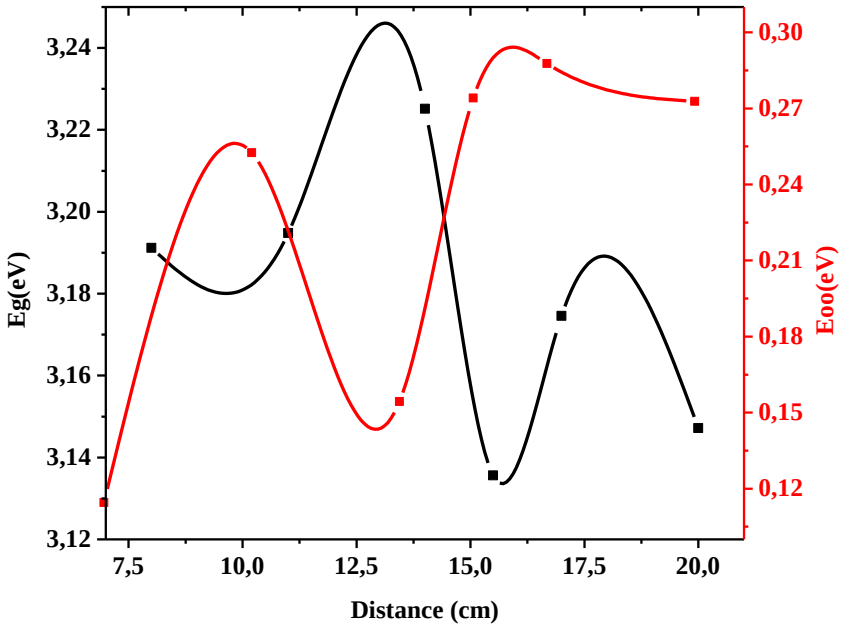

Figure.3.12: *Variation of energy gap and Urbach energy for different distances nozzle-substrate.*

Discussion:

The effect of nozzle-to-substrate distance resembles the effect of temperature in type of deposition process that occurs during spray. With the increase in nozzle-to-substrate distance the decomposition of precursors happens is similar to the increase in temperature and the processes change from (A) to (D) as we shown in Fig.2.2. The thickness of films increases with the decrease in nozzle-to-substrate distance due to the increase in droplets density.

From the results of this part we can deduce that the optimum nozzle-to-substrate distance which exhibits the best structural, optical and electrical proprieties is approx-imately 15.5cm. In the next experiment we adjust the distance at this value.

III.2.3. Effect of Air Pressure:

In order to study the effect of air pressure on ZnO thin film proprieties we prepared 8 samples at different air pressure values, the spray condition of this series are summarized in Table 3.1.

The effect of air pressure on the structural proprieties is presented in Fig.3.13. All samples shows the ZnO wurtzite polycrystalline structure with preferred orientation along (0 0 2) at $2\theta \approx 34.5°$. The intensity of this principal peak increases with increasing the air pressure, and other secondary peaks appear for pressures 0.3 and 0.35 bar at 2θ= 31.85°, 36.25°, 47.56°, 56,52°, 62,85°,67.98° and 72.56° for these orientations (100), (101), (102), (110), (103), (112) and (004) respectively. These changes could be attributed to the increasing in film thickness with increasing in air pressure values.

The changes of FWHM and stresses at different air pressure values are presented in Fig.3.14. We observe that FWHM of the principal peak (002) decreases from 0.172° to 0.142° after that it increases to 0.182° for these air pressure values respectively.

The stress values increases from 0.32 to 1.67 Gpa with increasing in air pressure values until the value 0.25 bar. FWHM and stress spectra show that the optimum air pressure value is 0.15bar.

The changes in both air pressure values 0.3 and 0.35bar could be attributed to the rise in the amplitude of ultrasonic waves from 65% to 85%.

The figure.3.15 shows the measured transmittance spectra as a function of the wavelength in the range 300-800 nm for films deposited at various air pressure values. The optical transmittance in the visible region for all films reduce greatly with decrease in wavelength, but we can deduce that is increasing from 40% up to 60-80% with increasing the air pressure until the value 0.15 bar, after that it decreases less than 20% with increasing the air pressure. This could be attributed to the changing in structural proprieties.

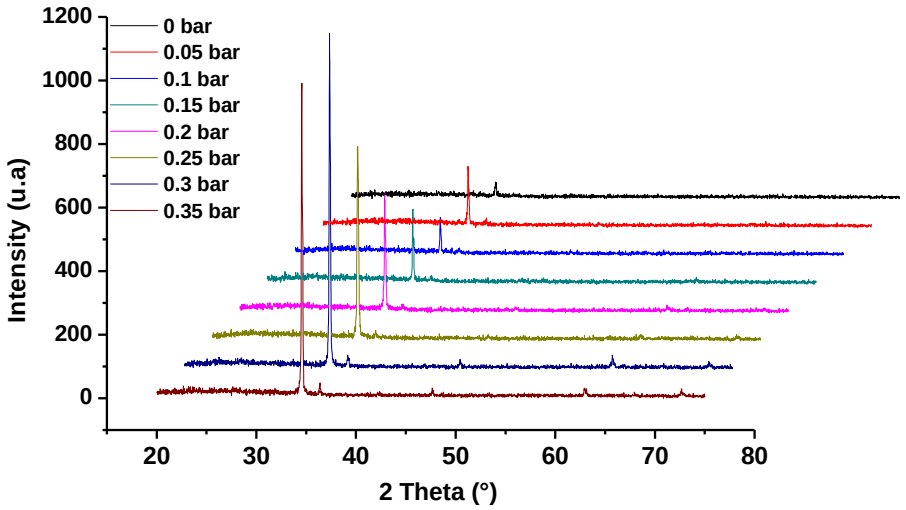

Figure.3.13: *XRD spectra of films deposited at different air pressure values.*

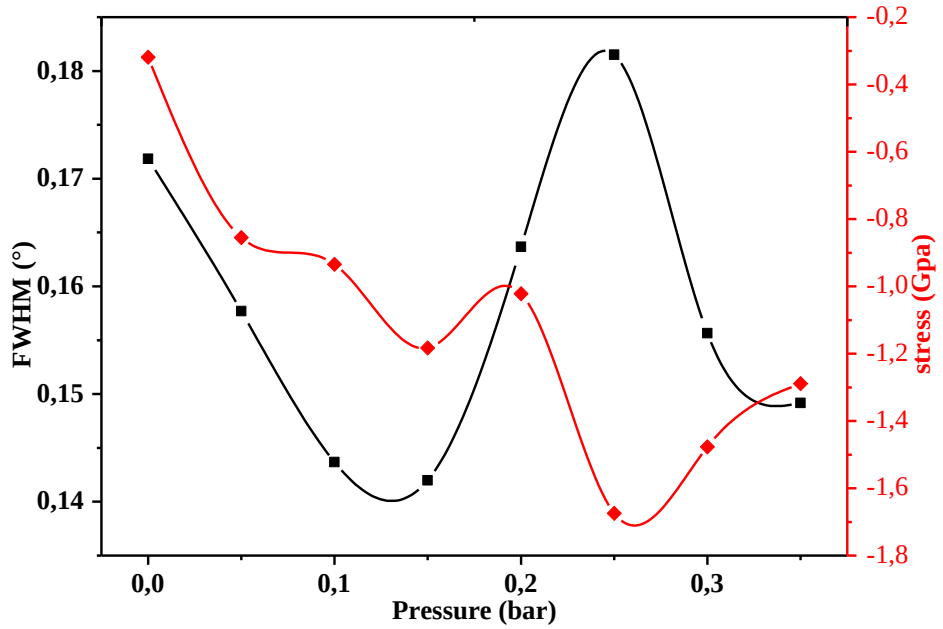

Figure.3.14: *FWHM and stress variations vs. air pressure variations.*

The energy gap and Urbach energy changes versus the air pressure changes are presented in the figure 3.16.With the increase in air pressure the energy gap values show an increase from 3.06 to 3.12 eV for 0.1bar, after that it decreases to 3.03 eV and 3.06 eV. Urbach energy shows a decrease from 0.54 to 0.31 eV with the increase in air pressures from 0 to 0.15bar, after that it increases to 0.45 eV with the increase of air pressures. The broadening in energy gap is accompanied with the decrease in disorder and with the improvement in the crystallinity and vice versa.

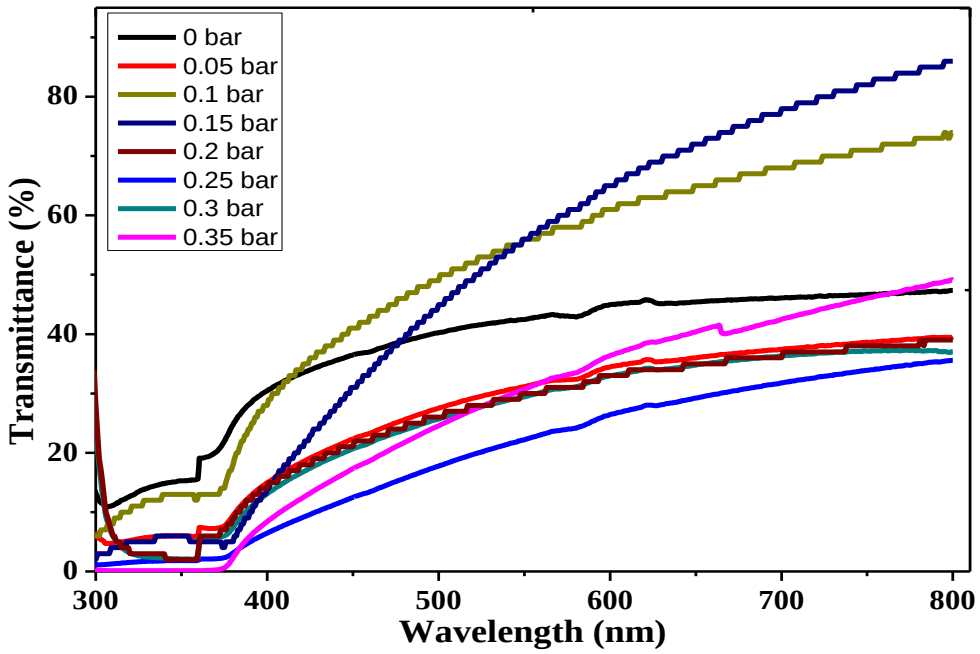

Figure.3.15: *Optical transmittance spectra for films deposited at different air pressures.*

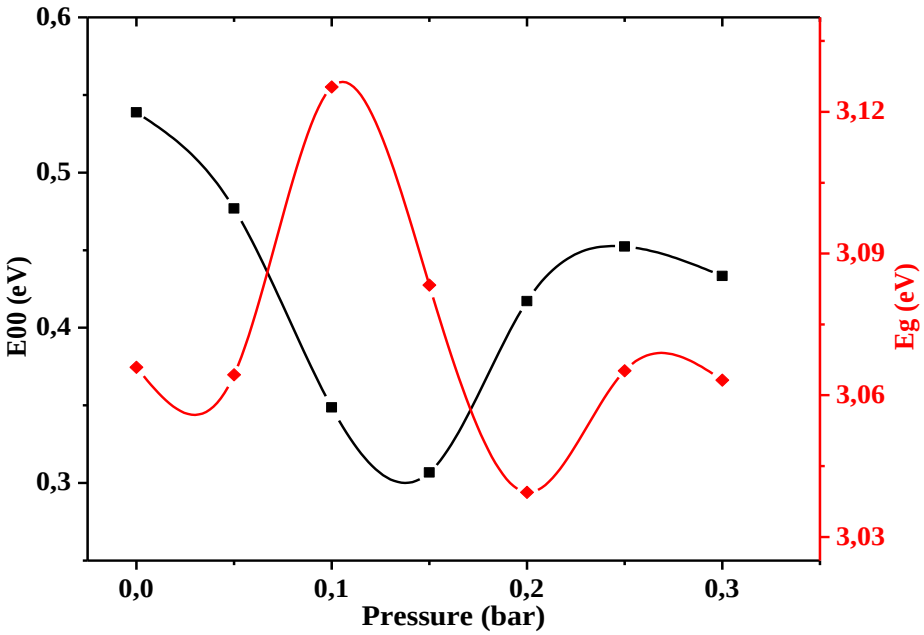

Figure.3.16: *Variation of energy gap and Urbach energy for different air pressure values.*

The electrical conductivity characterization of samples deposited at different air pressures was carried out by Van der Pauw technique. These electrical values are presented in Fig.3.17. For pressures 0bar and 0.1bar the electrical conductivity is lower than 10^{-6} $(ohm.cm)^{-1}$. With increasing the air pressure from 0.15 to 0.25 bar the electrical conductivity decreases from $2.2*10^{-4}$ to $5.1*10^{-5}(ohm.cm)^{-1}$. For both pressures

0.3 and 0.35 bar the increase in the electrical conductivity until 10^{-3} $(ohm.cm)^{-1}$ could be attributed to the increase in the ultrasonic wave amplitude.

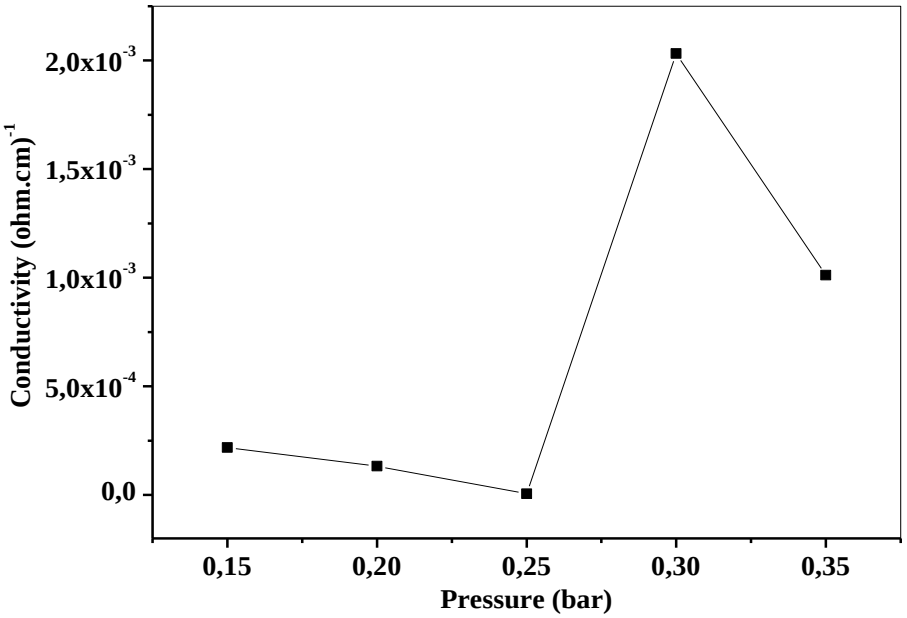

Figure.3.17: *Variation of conductivity vs. variation of air pressure values.*

Discussion:

The effect of the air pressure is also similar to the deposition processes which are illustrated in Fig .2.2. With the increase in air pressure the speed of droplets increase, then the decomposition of precursors take less time, therefore the decomposition process changes from (D) to (A).

By increasing air pressure the atomizer doesn't have enough time to divide the solution, therefore the size of droplets increases, and the spread of droplets decreases, then the density of droplets increases, therefore the film thickness increases.

From the results of this experiment we can deduce that the optimum air pressure which gives the best structural, optical and electrical proprieties is approximately 0.15bar.

GENERAL CONCLUSION

General Conclusion

The present work was based on the realization of ultrasonic spray pyrolysis system, the adjustment and the optimization of its parameters; by using the zinc oxide as a sample to achieve that.

We presented the way which used to improve ultrasonic spray by combination with pneumatic spray pyrolysis system and to adjust the flow rate of solution.

The effect of main deposition parameters which are: flow rate of solution, atomizer to substrate distance and air pressure on the structural, optical and electrical characteristics of zinc oxide thin films has been investigated.

The X-ray diffraction showed good crystallinity where most films have wurtzite polycrystalline structure with preferred orientation (002) with mean grain size reaches until D=550°A.

The images obtained by scanning electron microscope (SEM) present that the surfaces have good uniformity. And the EDX analysis demonstrates purity in chemical composition and non-stoicheometric films.

From uv-visible spectroscopy for optical properties we found that: the optical transmittance can attain high values about 80 % in the visible range of electromagnetic spectrum and the energy gap values varies in the range 3.1-3.27 eV.

Electrical measurements carried out by means of either two points and four points (van der Pauw) methods showed that the electrical resistivity is about $10^2\ \Omega$.cm for optimum values.

The results showed that the optimum values of the studied parameters are around: 0.5 ml/min of flow rate, 15 cm of atomizer-substrate distance and 0.15 bar of air pressure.

In the end, these results are in good agreement with other results in literature obtained by different spray deposition systems.

BIBLIOGRAPHY

BIBLIOGRAPHY

[1] K. Baedeker. Ann. Phys., 22 (1907) 749–766.

[2] G. Rupprecht. Zeitschrift fur Physik, 139 (1954) 504–517.

[3] G. Haacke. Ann. Rev. Mater. Sci., 7 (1977) 73–93.

[4] T. Minami. MRS Bull, 25 No.8 (2000) 38–44.

[5] B. G. Lewis and D. C. Paine. MRS Bull, 25 No.8 (2000) 22–27.

[6] T. Minami et al. Semicond. Sci. Technol., 20 (2005) 35–44.

[7] Q. Zhou et al. Materials Letters, 61 (2007) 531–534.

[8] H. Sato et al. Thin Solid Films, 236 (1993) 27–31.

[9] H. Kawazoe et al. Nature, 389 (1997) 939–942.

[10] H. Hosono. Thin Solid Films, 515 (2007) 6000–6014.

[11] J. L. Vossen et al, Physics of Thin Films, Academic Press, New York, (1977).

[12] Haacke, Ann. Rev. Mater. Sci., 7(1977)73-93.

[13] K. L. Chopra, S. Major and D.K. Pandya, Thin Solid Films, 102 (1983) 1-46.

[14] N. Mott, Conduction in non-crystalline materials, Oxford science publication, 1987.

[15] N. Mott, Metal-insulator transitions, Taylor & Francis, 1990.

[16] S. Rahmane, Elaboration and characterization of thin films by spray pyrolysis and magnetron sputtering, Doctorate thesis, University of Biskra, Algeria, 2008.

[17] R. G. Gordon. MRS Bull, 25. No. 8 (2000) 52–57.

[18] K. Ellmer, Journal of applied physics, 33, (2000) 17.

[19] K. Ellmer, A. Klein and B. Rech, Transparent conductive oxide, Springer, 2007.

[20] Ü. Özgür et al, Journal of applied physics, 98, (2005) 41301.

[21] J. Y. Seto, Journal of Applied Physics, 46 (1975) 5247.

[22] J. W. Orton, M. J. Powel, Rep. prog. phys., 43 (1980) 81.

[23] J.W. Orton, Thin solid films, 86 (1981) 351.

[24] E. Hecht, Optics, 2nd edition, ISBN 0-201-11611-1, Adelphi University, New York, 1987.

[25] P. Drude, Annal in Phys., 1, (1900) 566.

[26] R. J. Hong et al. J. Vac. Sci. Technol., 20 (2002) 900.

[27] M. Losurdo et al, J. Vac, Sci. Technol., 20 (2002) 37.

[28] I. Volintiru, M. Creatore and M. Van de Sanden, Journal of applied physics, 103 (2008) 033704.

[29] S. Logothetidis et al, Thin solid films, 516 (2008) 1345.

[30] J. Steinhauser, low pressure chemical vapor deposited zinc oxide for silicon thin film solar cells, Doctorate thesis, University of Neuchâtel, Switzerland, 2008.
[31] K. Ramamoorthy et al. Current Applied Physics, 6 (2006) 103–108.
[32] A. Walsh et al. Physical Review, 78 (2008) 075211.
[33] D. O. Scanlon and G. W.Watson, Chem. Mater, 21 No. 22 (2009) 5435–5442.
[34] C. R. Brundle, C. A. Evans and Jr. S. Wilson, Encyclopedia of Materials Characterization, Manning Publications Co**,** Greenwich, USA, 1992.
[35] M. Leszczynski, Common crystal structure of the group III-nitrides, EMIS Datareviews, The Institution of Electrical Engineers, Stevenage, UK, 1999.
[36] Z. H. Wang et al, Materials Letters, 63 (29) (2009)2533-2535.
[37] A. Janotti and C.G. Van de Walle, Applied Physics Letters, 87**(**2005)122102.
[38] T. Tomita et al, Applied Physics Letters, 87 (2005) 51911.
[39] C.G. Van de Walle, Defect analysis and engineering in ZnO, Elsevier, Netherlands, 2001.
[40] Y. Weifeng et al, Applied Surface Science, 255 (2009) 5669-5673.
[41] B. N. Pawar, S. R. Jadkar and M.G. Takwale, J. Phy. Chem. Soli., 66 (2005) 1779-1782.
[42] L. Shuang, and B. Xiaofang, Journal of Applied Physics, 104 (2008) 113533-113538.
[43] D. B. Zhong et al, Journal of Applied Physics, 101 (2007) 33713-33721.
[44] L. Castaneda et al, Journal of Physics: Condensed Matter, 18 (2006) 5105-5120.
[45] P. Kun Ho, K. Cheol, and M. Dae Young, Journal of Applied Physics, 81 (1997) 7764-7772.
[46] H. Ohta, et al, Applied Physics Letters, 76 (2000) 2740-2742.
[47] J. R. Bellingham, W. A. Phillips and C.J. Adkins, Journal of Materials Science Letters, 11 (1992) 263-265.
[48] K. H. Seong et al, Applied Physics Letters, 88 (2006) 202108-202121.
[49] Y. Yanfa, M. M. Al-Jassim and W. Su-Huai, Applied Physics Letters, 89 (2006) 181912-181921.
[50] A. Krtschil, et al, J. Physica, B 376 (2006) 703-706.
[51] C. H. Park, S.B. Zhang and W. Su-Huai, Condensed Matter and Materials Physics, 66 (2002) 073202-073211.
[52] J. G. Lu et al, Applied Physics Letters, 88 (2006) 222114-222121.
[53] S. Y. Huang et al, Materials Letters, 63 (2009) 972-974.
[54] A. Moustaghfir, Elaboration and characterization of ZnO thin films application in photo-protection of polycarbonate, Doctorate thesis, University of Blaise Pascal, France, 2004.
[55] W. Li et al, Nucl. Instrum. Methods. Phys. Res., B169 (2000) 59.
[56] P. Fons et al, Journal of Crystal Growth, 201 (1999) 627.

[57] H. B. Abdulhamid, Fabrication structural and electrical characteristics of ZnO thin films by direct current sputtering, University of Sains, Malaysia, 2009.

[58] F. Hamdani et al,J. Appl. Phys., 83 (1998) 983.

[59] S. Basu and A. Dutta, Mater. Chem. Phys., 47 (1997).

[60] P. Mitra, A. P. Chatterjee and H. S. Maiti, Materials Letters, 35 (1998) 33.

[61] A. P. Chatterjee, P. Mitra, and A. K. Mukhopadhyay, J. Mater. Sci., 34 (1999) 4225.

[62] J. Muller and S. Weissenrieder, Fresenius J. Anal. Chem., 349 (1994) 380.

[63] N. Koshizaki and T. Oyama, Sens. Actuators, B 66 (2000) 119.

[64] T. Dietl et al, Science, 287 (2000) 1019.

[65] X. J. Huang and Y. K. Choi, Sens. Actuators, B 122 (2007) 659.

[66] J. Goldberger et al, Journal of Physics and Chemistry, B109 (2005) 9.

[67] M. H. Huang et al, Science, 292 (2001) 1897.

[68] M. Law et al, Nature and Matter, 4 (2005) 455.

[69] E. Galoppini et al, J.Phys. Chem., B110 (2006) 16159.

[70] W. L. Hughes and Z. L. Wang, Appl. Phys. Lett., 82 (2003) 2886.

[71] S. J. Pearton et al, Superlattices and Microstructures, 34 (2004) 3-32.

[72] J. R. Arthur. Specimen handling, preparation, and treatments in surface characterization, Plenum Publishers, New York, 1998.

[73] A. Z. Moshfegh et al. Proceedings of the International Workshop on Physics and Technology of Thin Films. World Scientific Publishing, USA, 2004.

[74] K. Seshan. Handbook of Thin Film Deposition: Processess and Technologies. 2nd edition,William Andrew Publishing, New York, 2002.

[75] Yi. Liu, Z.L. Wang and Ze. Zhang. Handbook of Nanophase and Nanostructured Materials: Vol. 1, Kluwer Acadamic, Plenum Publishers, New York, 2003.

[76] A.N. Banerjee and K.K. Chattopadhyay, Progress in Crystal Growth and Characterization of Materials, 50 (2005) 52–105,.

[77] M. Kitabatake, K. Wasa and H. Adachi. Thin Films Material Technology: Sputtering of Compound Materials, William Andrew Publishing, New York, 2004.

[78] C. A. Bishop, Vacuum deposition onto webs, films, and foils. William Andrew Publishing, New York, 2007.

[79] J. I. Pankove and T. D. Moustakas. Semiconductors and semimetals: Gallium Nitride (GaN) II, Academic Press, San Deigo, 1999.

[80] J. H. Park and T. S. Sudarshan, Chemical Vapor Deposition. ASM International, 2001.

[81] R. V. Coleman and K. L. Horovitz, Solid state physics. Academic Press, New York, 1974.

[82] H. O. Pierson, Handbook of chemical vapor depostion. Noyes Publications, New York, 1999.

[83] M. Haruna, H. Nishihara and T. Suhara, Optical integrated circuits, McGraw-Hill Professional Publishing, 1989.

[84] Y. Pauleau, Chemical physics of thin film deposition processes for micro- and nano-technologies, Kluwer Acadamic Publishers, Netherland, 2002.

[85] H. Mader, D. Widmann and H. Friedrich. Technology of integrated circuits. Springer-Verlag, Berlin, 2000.

[86] A. Busnaina, Nanomanufacturing handbook. Taylor & Francis Group, USA, 2007.

[87] L. E. Scriven. Mat. Res. Soc. Symp. Proc, 121 (1988) 717–729,.

[88] K. L. Chopra and S. R. Das, Thin film solar cells, Plenum Press, New York, 1983.

[89] D. Beckel et al, Journal of electroceramics, 16 **(**2006) 221-228.

[90] L. Gary, Journal of the American Ceramic Society, 76 (1993) 2707-2726.

[91] D. Perednis and L. J. Gauckler, Journal of Electroceramics, 14 (2005) 103–111.

[92] JC. Viguie, J. Spitz, Journal of the Electrochemical Society, 122 (1975) 585-588.

[93] S.B. Majumder et al, Materials Science and Engineering, B103 (2003) 16.

[94] A. Sanchez-Juareza et al, Thin Solid Films, 333 (1998) 196.

[95] V. Craciun et al, Appl. Phys. Lett., 65 (1994) 2963.

[96] K. Matsubara et al, Thin Solid Films, 422(2002) 176.

[97] Y. Kashiwaba et al, Thin Solid Films, 411 (2002) 87.

[98] S.H. Jeong and J.H. Boo, Thin Solid Films, 447 (2004) 105.

[99] J. Lee et al, Thin Solid Films, 515 (2007) 6094.

[100] J. G. Lu et al,J. Appl. Phys., 100 (2006) 073714.

[101] Jin Ma et al, Thin Solid Films 279 (1996) 213.

[102] Z. Sofiani, Contributions in the study of non-linear optical proprieties of nano particles of ZnO thin films, Doctorate thesis, Ibn Toufil University, France, 2007.

[103] A. Hafdallah, Study of doping in ZnO thin films Elaborated by Spray Ultarasonic, magister memo, University of Constantine, Algeria, (2007).

[104] J. I. Goldstein et al, Scanning Electron Microscopy and X-ray Micronalysis, 3rd edition, Plenum Press, New York, 2003 .

[105] J. Tauc, R. Gorigorovici and A. Vancu, Physica Status Solidi, A (1966) 15.

[106] J. A. Olley, Solid State Communications, 13 (9) (1973) 1437-1440.

[107] J. I. Pankove, Physical Review, 140 (6A) (1965) 2059-2065.

[108] D. Redfield, Physical Review, 130 (3) (1963) 914-918.

[109] L. J. Van der Pauw, Philips Tech. Rev, 20 (1958) 220-224.

[110] John B. Mooney, Raddin SB. Ann Rev Mater Sci. 12 (1982) 81-101.

[111] R. Ondo-Ndong et al, J.of crystal Growth, 255 (2003) 68.

[112] R. Ayouchi et al, Thin Solid Films, 426 (2003) 68-77.

[113] H. Kim et al, Thin Solid Films, 377 (2000) 798-802.

[114] D. Zaouk et al, Microelectronics Journal, 37 (2006) 1276-1279.

[115] Nguyen Quang Tien, Do Thanh Dat and Pham Van Nho, Journal of the Korean Physical Society, 52 (2008) 1594-1597.

[116] Jérome Garnier et al, Thin Solid Films, 518 (2009) 1129-1135.

ABSTRACT:

The aim of this work is the deposition and the characterization of zinc oxide thin films in order to optimize an ultrasonic spray pyrolysis deposition system. We realized our deposition system by combination of ultrasonic spray technique with a pneumatic spray technique. The motivation for use this technique is its simplicity and effectiveness of preparation. The optimization of this deposition system was accomplished by studying the effect of the deposition rate, nozzle-to-substrate distance and air pressure on the structural, the optical and the electrical proprieties of ZnO thin films.

RESUME :

Ce présent travail a pour l'objectif de la déposition et la caractérisation des couches minces d'oxyde de zinc en vue d'optimisation d'un system de déposition par spray ultrasonique pyrolyse. Nous avons réalisé un système de dépôt par le technique spray ultrasonique combiné avec un spray pneumatique. La motivation d'utiliser cette méthode est sa simplicité et son efficacité. Des séries de film de ZnO ont été élaborés en variant le flux de la solution, la distance atomiseur-substrat et la pression de l'air, pour atteindre aux conditions idéales de notre système de déposition.

الملخص :

يهدف هذا العمل إلى ترسيب طبقات رقيقة من أكسيد الزنك من أجل تحسين نظام الرش بالموجات فوق الصوتية . حيث قمنا بدمج طريقة الرش بواسطة تكنولوجيا الموجات فوق الصوتية مع طريقة الرش بالهواء المضغوط . الدافع لاستخدام هذه التقنية هو بساطتها وفعاليتها ، وقد تم تحضير سلسلة من أفلام أكسيد الزنك لدراسة تأثير : التدفق،المسافة مذرر-حامل العينة و ضغط الهواء قصد الوصول إلى الشروط المثلى التي تعطي أفضل الخصائص البنيوية و الكهروضوئية .